

**KERNFORSCHUNGSZENTRUM  
KARLSRUHE**

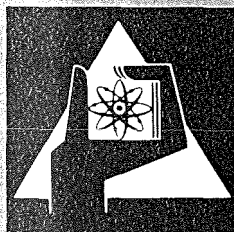
April 1977

KFK 2361

Institut für Neutronenphysik und Reaktortechnik  
Projekt Schneller Brüter

**Physics Investigations of Sodium-Cooled Fast  
Reactors:  
SNEAK-Assembly 9C**

compiled by: W. Scholtyssek  
with contributions from  
R. Böhme, P. Fehsenfeld, E. A. Fischer  
H. Giese, F. Helm, U. v. Möllendorff



**GESELLSCHAFT  
FÜR  
KERNFORSCHUNG M.B.H.**

**KARLSRUHE**

Als Manuskript vervielfältigt

Für diesen Bericht behalten wir uns alle Rechte vor

GESELLSCHAFT FÜR KERNFORSCHUNG M. B. H.  
KARLSRUHE

KERNFORSCHUNGSZENTRUM KARLSRUHE

KFK 2361

Institut für Neutronenphysik und Reaktortechnik  
Projekt Schneller Brüter

Physics Investigations of Sodium-Cooled  
Fast Reactors:  
SNEAK-Assembly 9C

compiled by

W. Scholtyssek

with contributions from

R. Böhme, P. Fehsenfeld, E.A. Fischer,  
H. Giese, F. Helm, U. v. Möllendorff

Gesellschaft für Kernforschung mbH., Karlsruhe



## Abstract

The assemblies 9C completed the SNEAK 9 series of SNR specific criticals. The main objectives of 9C were

- study of the influence of high Plutonium isotopes on fast breeder core parameters
- check of the sector substitution method, in particular with respect to SNEAK 2 and possible future mock-ups for large fast breeder reactors
- study of the reactivity effect of coolant loss in large core zones
- study of the material worth of various absorber type materials, e.g. enriched Boron and Europium.

Two geometrically simple and similar criticals, one Uranium-fueled (SNEAK 9C-1), one Plutonium-fueled (SNEAK 9C-2), were designed to cover these points.

This report contains a detailed description of the SNEAK 9C-assemblies and of experiments related to core physics and to neutron physics parameters of the compositions used. The results of the experiments are compared to calculations carried out mainly with Karlsruhe code systems and the KFKINR cross section set. Only in some cases other cross sections were used.

The work covered by this report was performed in close cooperation between the Gesellschaft für Kernforschung and the industrial consortium for the SNR. Part of the work was enabled by UKAEA, which supplied GfK with 80 kg of Plutonium enriched in  $^{240}\text{Pu}$ .

## Physikalische Untersuchungen von schnellen natrium-gekühlten Reaktoren, SNEAK-Anordnung 9C.

### Zusammenfassung

Mit den Anordnungen 9C wurde die SNR-spezifische SNEAK-9-Serie von kritischen Cores vorläufig abgeschlossen. Wesentliche Ziele von SNEAK-9C waren

- Untersuchung des Einflusses von höheren Plutoniumisotopen auf Schnellbrütercoreparameter
- Überprüfung der Sektorsubstitutionsmethode, besonders im Hinblick auf SNEAK-2 und mögliche zukünftige Mock-ups großer Brutreaktoren
- Untersuchungen zum Na-Void Effekt
- Untersuchungen zum Materialwert verschiedener Absorbermaterialien, z.B. angereichertem Bor und Europium.

Zur Abdeckung dieser Punkte wurden zwei geometrisch einfache kritische Anordnungen gebaut, ein Urancore (SNEAK-9C-1) und ein Plutoniumcore (SNEAK-9C-2).

Der vorliegende Bericht enthält eine ausführliche Beschreibung der 9C-Anordnungen sowie eine Zusammenstellung der mehr physikalisch orientierten Experimente in den Cores. Die experimentellen Ergebnisse werden mit Rechnungen verglichen, die mit Karlsruher Code Systemen und dem KFKINR Querschnittsatz durchgeführt wurden. In einigen Fällen wurden andere Querschnitte verwendet.

Die in diesem Bericht beschriebene Arbeit wurde in enger Zusammenarbeit zwischen der Gesellschaft für Kernforschung und dem Industriekonsortium für den SNR durchgeführt. Ein Teil der Arbeit wurde durch die UKAEA ermöglicht, die 80 kg Plutonium, angereichert mit  $^{240}\text{Pu}$ , leihweise zur Verfügung stellte.

## Table of Contents

	Page
1. Introduction	1
2. Description of the Assemblies	3
2.1 SNEAK 9C1	3
2.2 SNEAK 9C2	4
2.3 Central Substitutions	5
3. Analysis of Critical Experiments	8
3.1 Experiments	8
3.2 Computational methods	8
4. Reaction rate measurements	12
4.1 Fission rate distributions by fission chambers	12
4.2 Reaction rate traverses by the activation technique	13
4.3 Cell averaged reaction rates	16
4.4 Fission reaction rates of higher actinides	21
5. Material buckling determination	22
6. Material worth measurements	24
6.1 Experiments	24
6.2 Calculations	25
6.3 Results and Conclusions	26
7. Reaction rate balance in SNEAK 9C1 and 9C2	27
8. Determination of relative actinide (1+ $\alpha$ ) values	28
9. Measurements of $\beta_{eff}$ in SNEAK 9C1 and 9C2	30
9.1 Measurement with a calibrated $^{252}\text{Cf}$ Source	30
9.2 Measurement by the Pile Oscillator Technique	32
9.3 Results and Conclusions	32
References	33
List of tables	36
List of figures	37

## 1. Introduction

The SNEAK \*) 9 series /1/ of critical experiments was basically designed to improve the prediction of neutronic, engineering and safety parameters for the German BeNeLux fast breeder prototype SNR 300.

The main objectives were determination of

- fuel enrichment
- control rod enrichment
- power distribution
- maximum sodium void effect
- breeding ratio

of the SNR. Three different assemblies were necessary to cover all these parameters adequately.

SNEAK 9A /2,3/ was a geometrically close mock-up of the SNR, including control rods, but  $^{235}\text{U}$ -fueled rather than plutonium-fueled because of the limited amount of plutonium at SNEAK. 9A gave detailed information about the power distribution in a SNR type core at different rod positions.

SNEAK 9B /4/ was designed to simulate the inner zone of the SNR yielding information about the axial breeding ratio, maximum sodium void effect and other parameters.

Problems still open were

- Influence of higher Pu isotopes on the prediction of fast breeder core parameters. The SNR-type plutonium will differ considerably in its  $^{240}\text{Pu}$  and  $^{241}\text{Pu}$  content from that of SNEAK stock rising additional uncertainties in the transfer of SNEAK experiments to SNR parameters.

---

\*) Schnelle Null Energie Anlage Karlsruhe  
(Zero Power Reactor at Karlsruhe)

- Validity of the sector substitution method applied in SNEAK 2 /5/, on which the  $k_{\text{eff}}$ -prediction of the SNR is based to a great extent.
- Validity of computational methods to calculate the sodium void effect. The good agreement between calculation and experiment found in SNEAK 9B was to be confirmed by complementary measurements in a core with a different neutron spectrum and flux shape.

To study these problems, geometrically simple critical configurations were designed. The reference core, SNEAK 9C-2, was a one-zone pure  $\text{PuO}_2\text{UO}_2$ -sodium assembly. It was built by a  $360^\circ$  sector substitution out of a one-zone uranium core, SNEAK 9C-1, that had approximately the same geometrical and neutronic characteristics.

Three different central zones with "dirty" Plutonium (Plutonium with about 20 % of  $^{240}\text{Pu}$  in its isotopic vector) were substituted into the reference core 9C-2:

- a 30 ltr. zone with dirty plutonium in the form of  $\text{PuO}_2\text{UO}_2$  of SNEAK stock ("POS"-zone)
- a 80 ltr. zone with dirty plutonium metal of ZEBRA stock, combined with  $\text{Fe}_2\text{O}_3$  to simulate oxide fuel ("POZ"-zone)
- a 80 ltr. zone also with ZEBRA-plutonium metal, but combined with graphite to simulate carbide fuel ("C"-zone).

The 9C-program encompassed SNR-specific experiments as well as research work more generally applicable to reactor physics. This report deals mainly with the second category of experiments. A second report will cover the sodium void-, absorber- and substitution-experiments.

The experimental work on SNEAK 9C started in December 1973 and was completed in May 1975.

## 2. Description of the assemblies

### 2.1 SNEAK 9C-1

The 9C-series started with a geometrically simple Uranium-Sodium configuration, SNEAK 9C-1. It was a one zoned core with a height of 60 cm and a radius of  $\sim 36$  cm. The core was surrounded by a 30 cm thick blanket of depleted Uranium. The unit cell of 9C-1 was designed to match closely the neutronic characteristics of the Pu reference core SNEAK 9C-2 and was therefore somewhat complicated.

Fig. 1 a shows a cross section of the clean critical assembly. The core region consisted of 150 elements including the 12 SNEAK shim- and safety rods. The total element number (core + blanket) was 500.

Fig. 1 b shows the r-z diagram of the core. Heights and radii given refer to the geometrical model used for the r-z-diffusion-calculation (see section 3). A clean central zone with radius  $R_1 = 19.41$  cm (equivalent to 40 elements) was defined, while the control-rods were smeared over the outer core zone. The mixture numbers  $M_i$  refer to regions with uniform particle densities.

Table 1 contains the homogenized particle densities for all assemblies of the 9C-series.

Fig. 2 shows the cells used in SNEAK 9C-1. The core element contained 16 normal cells. The loading of four elements (position 15/26, 15/13, 20/26 etc. of Fig. 1) was split along a vertical plane into core and blanket material. The core half of these elements consisted of two layers of vertically oriented core cells as shown in fig. 2 b, depleted Uranium blocks filled the blanket half of the elements. Thus minimum excess reactivity of the critical core at full core symmetry was reached. For the radial channel the two central cells were substituted by a window cell. The control rod cell is built of small SNEAK platelets (edge length = 46 mm). All 9C assemblies had the same control rod loading. Special cells, e.g. for foil measurement, pile oscillator or other experiments will be described in the corresponding sections of this report.

For the radial and axial blanket SNEAK rodlets of depleted uranium were used. The rodlets have a square cross section, a bundle of 3 by 3 fits into a SNEAK element.

## 2.2 SNEAK 9C-2

SNEAK 9C-2 was built by a complete sectorwise substitution of the 9C-1 uranium fuel by Plutonium fueled elements. The resulting core was the first single zoned Plutonium Sodium configuration in SNEAK. Fig. 3 shows cross section and r-z-diagram of the critical assembly. The number of core elements was 139, the control rod loading and arrangement and the outer blanket border were kept the same as in 9C-1. The normal cell of 9C-2 was very simple: 1  $\text{PuO}_2\text{UO}_2$  mixed oxide platelet, 1 Na platelet. It is shown in fig. 4 together with the window cell for the radial channel. A core element contained 48 normal cells. A window cell substituted 2 normal cells in the core midplane.

## 2.3 Central substitutions

SNEAK 9C-2 was defined as the reference core for the central substitution of three different compositions with "dirty" plutonium (plutonium of high  $^{240}\text{Pu}$  content). The core cross sections of the respective critical assemblies and their r-z-diagrams are shown in fig. 5 and fig. 6. The unit cells are shown in fig. 7 a. Some special cells are presented in fig. 7 b and 7 c.

### 2.3.1 9C-2/POS

30 kg of dirty plutonium of SNEAK stock were substituted in a central zone of 32 ltr. volume. The zone had a square cross section (6 by 6 elements) and a height of 30 cm.

The platelets with dirty plutonium have the same dimensions and the same chemical components ( $\text{PuO}_2\text{UO}_2$ ) as the normal plutonium platelets. Moreover was the isotopic vector and the Pu:U ratio chosen in order to match closely the reactivity of normal SNEAK plutonium. The cell arrangement of the POS zone (fig. 7) was therefore the same as for the reference core, and no major finestructure or spectral effects are expected to influence the substitution experiment.

### 2.3.2 9C-2/POZ

80 kg of dirty plutonium on loan from Zebra (Winfrith, GB) were used to built a central zone of  $\sim 22$  cm radius at full coreheight, called POZ-zone. The cell structure of this zone differed strongly from that of the reference core, as the English fuel has a metallic consistency (plutonium alloyed with a small percentage of gallium), and the platelet height is only half of that

of the SNEAK plutonium platelet. Thus a complicated cell of more than 50 mm height had to be designed to match the neutronic characteristics of the 9C-2 composition (fig.7a). Fine structure effects are not negligible in this case.

As no English platelets with holes were available, a channel element for axial traverses had to be built with vertically oriented platelets. Fig. 7b and 7c show the cell arrangements for channel elements.

No chamber traverses were carried out in 9C-2/POS as in this case the test zone was too small for an accurate buckling measurement.

### 2.3.3 "Carbide"-zone (9C-2/C)

The metallic, oxygen free state of the ZEBRA plutonium enabled the construction of a zone simulating a carbide fuel reactor environment. This was realized in 9C-2/C. The cell of the C zone was arranged in such a way that the particle densities were close to those of POZ with exception of oxygen. This was substituted by graphite with an atomic density about half of that of oxygen in POZ corresponding to the respective stoichiometry of carbide and oxide fuel. The resulting cell structure is shown in fig. 7 a, cells for channel elements in fig. 7 b and 7 c.

#### 2.3.4 The "copper" zone' 9C-2/Cu

The English plutonium platelets consist of a plate of plutonium gallium alloy, installed within a double cladding. The outer cladding is made from steel, the inner cladding from a 0.127 mm thick copper foil. Gallium and copper are materials not used in SNEAK before. This gave rise to the assumption that the accuracy of the analysis of experiments performed in 9C-2/POZ and 9C-2/C might suffer from the not well known neutronic properties of these materials. It was therefore suggested to built a zone in SNEAK 9C-2 containing copper, because of its easy availability and major contribution by weight, in combination with mixed oxide fuel of SNEAK stock.

The cell of this zone, called the Cu-zone, consisted of the normal 9C-2 cell, one sodium and one  $\text{PuO}_2\text{UO}_2$  platelet, with a copper foil of 0.1 mm thickness inbetween. The zone had a square cross section of 6 x 6 elements. The height was  $\sim 30$  cm, extending over the central 24 cells of an element. The experiments in this zones comprised reaction rate measurements, central sodium void and determination of critical mass.

### 3. Analysis of Critical Experiments

#### 3.1 Experiments

The "clean critical" assemblies were built with the minimum number of core elements necessary to reach the critical condition. The remaining excess reactivity was compensated by calibrated SNEAK shim rods. In all cases the excess reactivity was less than  $0.1 \% \Delta k/k$  - the worth of one edge element was about  $0.12 \% \Delta k/k$ . Core cross sections and r-z-diagrams are shown in fig. 1 and 3 of 9C-1 and 9C-2, respectively, and in fig. 5 and 6 of the substitution assemblies POS, POZ and C.

#### 3.2 Calculational method

The basic calculation was carried out by the 2-dim. diffusion code DIXY /6/ in r-z-geometry. 26 group cross sections from the KFKINR /7/ set were used. The mesh-size was chosen to 1 cm throughout the core region and 2 cm in the blanket. Material dependent fission neutron spectra of the central test regions, calculated by NUSYS module 2296, were used.

The SNEAK control rods, filled with uranium, were homogenized over the outer core zone.

The following corrections were applied to the diffusion calculation results:

### 3.2.1 Transport correction

These corrections were determined by comparing 1-dim. transport calculations carried out by the code DTK /8/ in S8, to 1-dim. diffusion calculations done with the same meshsize and geometry. Axial and radial corrections were calculated independently, the total correction being the unweighted sum of both. In the case of 9C-2/POZ this procedure was checked by a 2-dim. transport calculation to the order S8 with the code SNOW /9/. The difference between both methods was  $\sim 0.1\%$ .

### 3.2.2 REMO correction

The REMO /10/ correction improves the 26 group elastic removal cross sections by weighting with the collision density spectra of the particular composition under investigation.

### 3.2.3 Heterogeneity

The heterogeneous distribution of fuel and structural materials was extensively treated with the cell program KAPER /11/ followed by diffusion calculations. In KAPER heterogeneity corrected cell averaged cross sections were produced. The cells were modelled in great detail, including the structure of the platelets themselves. This was important especially for the Zebra-plutonium platelets because of their metallic consistency and relatively thick canning compared to the fuel nucleus.

Results from DIXY r-z-calculations found with these cross sections were compared to results for a "quasihomogeneous" case where the KAPER cross sections used were derived from the homogenized composition introduced into two regions of typical platelet thickness (0.6 cm).

The heterogeneity correction for the effect of substituting zone POZ into the 9C-2 reference composition amounted to about 0.5 %. From this it is evident that the interpretation of the substitution experiments involving ZEBRA plutonium will suffer somewhat from the questionable accuracy and reliability of the applied heterogeneity correction.

It is also possible that streaming effects play an important role. As the geometric cell arrangement is repeated horizontally in each element throughout a zone of the same kind, layers of equal materials, e.g. sodium platelets, are extending over one region but not continuing into regions of different cell design, e.g. from 9C-2 to 9C-2/POZ. Thus streaming layers are interrupted at region borders. At present it is not possible to treat this effect theoretically, rising additional uncertainties in the interpretation of the substitution experiments.

#### 3.2.4 Cylindrization correction

The effects of cylindrization of the core and of homogenization of the uranium loaded SNEAK control rods in the 2-dim. r-z-diffusion calculation was taken into account by comparing a 2-dimensional X-Y-diffusion calculation to a 1-dimensional diffusion calculation in radial direction. The same axial group dependent bucklings were used in both cases.

### 3.2.5 Fission spectrum, correction

The DIXY code uses only one fission spectrum for all regions, in the present cases always the material dependent spectrum of the central test region. The correction applied accounts for the difference in the fission spectra of the outer zones to that of the central zone and is in all cases very small.

### 3.3 Comparison of experimental and calculational results

The experimental and calculated results of the critical assemblies are compiled in table 2. In the cases of the assemblies containing only materials of SNEAK stock the calculated overestimation of about 0.8 %  $\Delta k/k$  known already from the analysis of similar sized cores using KFKINR cross sections is observed again. Significantly lower is the overestimation of the assemblies with zones of Zebra stock. This is especially true if one considers, that the weight of the substitution zones is only about half of that of the full core.

The cause of this effect is not clear. Problems in treating the heterogeneity or streaming effects as discussed in section 3.2.3 may play a role. It is also possible that materials present in the Zebra platelets like copper and gallium, where only inaccurate or even no cross sections are existing, might influence the results.

#### 4. Reaction rate measurements

In this chapter the measurements of capture and fission reaction rates in fissile and fertile materials are reported. Reaction rate distributions were determined by fission chambers and by activation foils. Cell fine structure measurements combined with absolute fission fragment counting methods were performed in order to get cell averaged reaction rate ratios. Fission rates of higher plutonium and americium isotopes were investigated by specially developed miniature chambers. Most of the techniques applied were routine and are described elsewhere (e.g. /12/). Only new or improved methods are discussed in greater detail in this report.

##### 4.1 Fission rate distributions by fission chambers

For the determination of the material bucklings, of the normalization integrals and as a check for activation measurements, axial and radial fission rate traverses were performed in all of the assemblies with exception of 9C-2/POS. In this case the substitution zone was too small to get reliable results for a buckling evaluation with sufficient accuracy.

Commercial fission chambers with 6 mm diameter and 25 mm active length with fissile layers of  $^{237}\text{Np}$ ,  $^{235}\text{U}$ ,  $^{238}\text{U}$  and  $^{239}\text{Pu}$  were used. The cell structure of radial channel elements is shown in fig. 2 a (9C-1), fig. 4 (9C-2) and fig. 7 b (9C-2/POZ and 9C-2/C). Platelets with holes of 13 mm diameter were used to built an axial channel in 9C-1 and 9C-2.

No such platelets were available for the ZEBRA plutonium fuel. In this case, the axial channel was built by vertically orienting the platelets and using the same aluminium spacers as for the radial channel (see fig. 7 c). The amount of fuel remained the same in these elements, but sodium was partly replaced by aluminium.

The axial measurements were carried out with the double chamber system originally introduced for power scanning purposes in SNEAK 9A /13/. Radial traverses were done with the normal single chamber system.

#### 4.2 Reaction rate traverses by the activation technique

The distribution of fission rates of the principal isotopes and of capture rates of  $^{238}\text{U}$  have been measured by the activation technique. Enriched and depleted metallic uranium foils of 0.1 mm thickness and 25 mm diameter have been used. Plutonium fission rate traverses were measured by foils of plutonium-aluminium alloy about 0.5 mm thick with a diameter of 9.5 mm. The foils were positioned in the cells either between platelets or inside special platelets with holes, filled with filling pieces of the platelet material to avoid perturbation of the neutronic environment. Axial distances of measurement points were chosen as multiples of cell heights. Thus a modulation of the global distribution by fine structure effects of the cell is avoided, but it must be taken into account that the cell fine structure itself might vary somewhat due to neutron spectral changes, going from the core center to the core blanket border. It must also be taken into account that the measurement point selected in the cell is normally not representative for the cell average values of the reaction rates. This is important if the traverse crosses the border of regions with different cell configurations, e.g. core and blanket. The latter, consisting of depleted uranium only in the 9C assemblies, can practically be viewed as homogeneous. Thus "average" values are given directly in the blanket regions if one neglects perturbation by the foils themselves.

For activation the foils were wrapped into 10  $\mu$  thick aluminium sheets to avoid parasitic capture of fission fragments escaping from neighbouring fissionable materials of platelets or other activation foils.

After activation the foils were analyzed in an automatic foil changer. For fission rates, the integral  $\gamma$ -activity above 630 keV was recorded in several cycles. The sequences of foils was reversed after each cycle to eliminate the time dependency of the  $\gamma$ -activity. Na J (Tl)-crystals were used as detectors. The raw data were corrected for background, dead time losses and contribution of others than the main isotope in the foil (e.g. of  $^{235}\text{U}$  fission in depleted uranium targets).

$^{238}\text{U}$  capture rates were measured by counting the 277 keV  $\gamma$ -line of  $^{239}\text{Np}$  emitted by activated depleted uranium foils with a Ge(Li) detector.

The accuracy of relative reaction rate data is mainly determined by statistical errors. Minor contributions arise from other sources like isotopic corrections,  $\gamma$ -selfabsorption, dead time correction and so on. Typical total errors (1 $\sigma$ ) are 0.5 % in the core region, rising up to 1.5 % in the outer blanket zones where fluences were low.

Examples of fission rate distributions resulting from activation measurements in the reference core SNEAK 9C-2 are shown in figures 8 a - c and 9 a - c.  $^{238}\text{U}$  capture rate traverses are shown in fig. 8d and 9d.

They are compared to theoretical distributions calculated by the DIXY diffusion code and KFKINR cross sections, and to experimental results from fission chamber measurements.

Generally one can state, that a good agreement exists between calculated and experimental results in the core region. A slight shift of the symmetry axis to negative values is observed for the activation foil data. This stems from a small but not negligible asymmetry in fuel loading relative to the core midplane as a result of the asymmetric cell design, sodium in the upper half and the mixed oxide fuel in the lower half of the cell.

The agreement becomes poorer in the outer zones of the core. Here the diffusion theory reaches the limits of its validity especially for reactions with strong neutron energy dependence, e.g. fission of  $^{238}\text{U}$ .

### 4.3 Cell averaged reaction rates

The accurate knowledge of reaction rates of the fissile and fertile materials of an assembly is highly important in terms of evaluation of the neutron balance, of spectral characterization and others. Measurements of cell averaged fission reaction rates of  $^{235}\text{U}$ ,  $^{238}\text{U}$  and  $^{239}\text{Pu}$  and of  $^{238}\text{U}$  capture rates were therefore performed in all 9C assemblies with great care.

The problem is twofold. First the reaction rate fine structure across a cell, generated by the heterogeneous distribution of fissile, fertile and structural materials, has to be determined. Secondly absolute values of fission and capture rates have to be measured.

#### 4.3.1 Fine structure measurements and calculations

For fine structure measurements a method is applied based on the activation technique. Activation foils are inserted in special fuel platelets with holes, the remaining space being filled with pellets or filling foils of the same composition as the platelet. Thus only small amounts of materials originally not present in the cell are introduced. Fig. 10 shows as an example the experimental arrangement of the fine structure measurement in the cell of SNEAK 9C-2/POZ. Metallic and oxide foils were used to determine the fine structure in the  $\text{UO}_2$  platelets. The composition of the platelet was simulated as closely as possible, including steel covers of the holes in substitution of the original steel cannings. No english plutonium platelets ("PuE" in fig. 10) with holes were available. As they contained only very small amounts of  $^{238}\text{U}$ , their contribution to the cell averaged reaction rates of  $^{238}\text{U}$  fission and  $^{238}\text{U}$  capture could be neglected. On the other hand the fine structures of  $^{235}\text{U}$  and  $^{239}\text{Pu}$  fission are very small and measurements of the rates outside the main fuel platelet were sufficient for determination of cell averaged rates in this case. Similar arrangements as shown in fig. 10 were designed for cell measurements in other 9C-assemblies.

Fig. 11 - 15 show the fine structure of  $^{238}\text{U}$  fission and  $^{238}\text{U}$  capture reaction rates in the 9C assemblies.

The experimental results are compared to calculations performed with the cell code KAPER using KFKINR cross sections. The geometrical model included the axial material distribution of the platelets themselves. Radially the material was smeared over the fuel element cross section. The leakage was accounted for by using group dependent axial (vertically to the platelet structure) and radial (parallel to the platelet structure) bucklings.

The conclusions that can be drawn confirm observations already made in earlier experiments (assemblies SNEAK 9A and 9B). Firstly the  $^{238}\text{U}$  fission fine structure is calculated remarkably well. Even in cases with strong heterogeneity resulting in fine structure effects up to 15 % across a cell (9C-2/POZ and 9C-2/C) are the deviations between calculation and experiment in the order of 1 % or less.

Secondly there are significant discrepancies between calculation and experiment in the case of  $^{238}\text{U}$  capture fine structure. Although the shape of the fine structure shows the right trend, its strength is significantly underestimated by calculation. A factor of 1.5 - 2 is found in some cases between measured and calculated structure across a platelet.

#### 4.3.2 Absolute fission and capture rates. Averaged spectral indices

##### a) absolute fission rates

The absolute scaling of activation foil measurements is achieved by irradiating foils not only in the cell but also between well calibrated fission fragment counters. For this purpose sealed ionization chambers of the parallel plate type are used at SNEAK. They are equipped with thin layers of fissionable materials of well known mass and isotopic composition. The reference activation foils are positioned between the fissionable layers of two chambers, the distance of the layers does normally not exceed 1 mm. It is assumed, that the fission rates in the activation foils and in the layers are practically the same.

Table 3 shows characteristic data of the SNEAK standard chambers used during the irradiation experiments in the 9C assemblies. The layer masses given include all fissile isotopes. The mass of the Pu9-25 chamber has very recently been changed to the value quoted in table 3. The original value of 28.98  $\mu\text{g}$  was based on a low geometry  $\alpha$ -measurement using the  $^{239}\text{Pu}$  half life of 24370 y. In the meantime two new measurements by Oetting /16/ and Aleksandrov /17/ of the  $^{239}\text{Pu}$  half life have been published giving values of 24070 y and 24060 y respectively. These new values lead to the Pu9-25 mass of table 3.

The absolute masses of the chambers, including the new plutonium mass of the Pu9-25 chamber, are very well confirmed by inter-laboratory comparison work done at the  $\Sigma\Sigma$  neutron standard facility at Mol /14/ and at the National Bureau of Standards /15/. The agreement is in the 0.5 % range between NBS and GfK for all three chambers of table 3, and better than 1 % between Petten values and GfK. Thus it can be excluded that large systematic errors affect the accuracy of absolute fission rate measurements in SNEAK.

b) absolute  $^{238}\text{U}$  capture rates

Absolute  $^{238}\text{U}$  capture rates are determined by quantitative counting of the  $^{239}\text{Np}$ - $\gamma$ -activity of irradiated  $^{238}\text{U}$  targets. This is achieved by calibrating the Ge(Li)- $\gamma$ -detector with an  $^{243}\text{Am}$  source of known activity, determined by low geometry  $\alpha$ -counting. The potential accuracy of this method is 1 - 1.5 %. The above mentioned intercalibration effort /14/ has shown that, although each laboratory claims a similar accuracy for its method, no agreement could be reached in the 3 % region. It is therefore stressed that further work should be invested to improve reliability in the value of this very important reactor parameter.

c) Results

The combination of cell fine structure and absolute rate measurement yields cell averaged reaction rates and rate ratios. Table 4 shows values for the central test regions in the SNEAK 9C assemblies. They are compared to results of cell- (KAPER) and homogeneous diffusion-calculations using KFKINR cross sections.

The errors given include calibration and statistical errors of chamber measurements and of foil measurements necessary for transfer of chamber results to cell averaged rates. In four assemblies (9C-1, 9C-2, POZ, C ) the reaction rates were measured twice each during different irradiations.

The reproducibility was better than 1 % for fission rates, but deviations up to 2 % were observed regarding  $^{238}\text{U}$  capture rate results. It is not clear up to now where this large deviations, exceeding considerably the sum of statistical errors in the applied method, come from. Use of activation foils of different sizes and materials - 12 mm and 25 mm diameter, oxide and metal - in the complicated cell configurations may play a role.

The comparison of experimental results to calculation shows the known discrepancy of about 10 % in the cross section ratio  $\sigma_f(^{238}\text{U})/\sigma_f(^{235}\text{U})$  and of more than 5 % in  $\sigma_f(^{239}\text{Pu})/\sigma_f(^{235}\text{U})$ .

Use of the cell code KAPER brings no significant improvement against homogeneous diffusion calculation. The difference also stays the same going from 9C-1, a purely uranium loaded core, to the 9C-2 assemblies, having plutonium-uranium oxide or carbide loadings.

The C/E values of the cross section ratio  $\sigma_c(^{238}\text{U})/\sigma_f(^{235}\text{U})$  are in the order of 1.0 with deviations of  $\sim 3.5$  % to both sides. This gives a variation of the C/E values far greater than those of the fission ratio. If one groups the 9C-assemblies in those with less (9C-2, 9C-2/POS and 9C-2/Cu) and more (9C-1, 9C-2/POZ and 9C-2/Cu) heterogeneous cells, the situation is somewhat improved. All "less heterogeneous" cores have C/E values higher than the average value 0.9942 (KAPER calculations are considered here), the "more heterogeneous" cores have values less than the average. This could indicate, that fine structure effects are not sufficiently taken into account by calculation, and that this is also the case for KAPER as it gives no significant improvements compared to the diffusion calculation. This is somewhat in line with the observation made throughout the 9C assemblies and also in earlier experiments (9B and 9A), that  $^{238}\text{U}$  capture fine structure effects are calculated significantly lower than measured. A more careful analysis of the situation both from the experimental and calculational side seems necessary.

#### 4.4 Fission reaction rates of higher actinides

Fission reaction rates of  $^{240}\text{Pu}$ ,  $^{241}\text{Pu}$  and  $^{241}\text{Am}$  were measured by fission chambers in the 9C-2-cell and in 9C-2/POS. For this purpose small ionisation chambers of 12 mm diameter and 6 mm height were developed. They could be inserted in special fuel platelets with holes. Fig. 16 shows the experimental arrangement in the reference core 9C-2.

The chamber housing is made of aluminium oxide with the active layer fixed at the steel bottom. The gas pressure is  $\sim 2$  atm. The effective masses of the active layers were determined by low geometry  $\alpha$ -counting and/or fission fragment counting relative to SNEAK standard chambers. Table 5 contains characteristic data of miniature chambers used in this experiments.

The chamber was positioned in the cell in such a way that the active layer was in close contact to a fuel pellet inside a fuel platelet (fig. 16). The empty space above the chamber ( $\phi$  12 mm x 18 mm) contained plug and cable.

The neutron spectrum perturbation caused by the experimental arrangement is not negligible regarding the threshold reactions  $^{240}\text{Pu}$  and  $^{241}\text{Am}$ -fission.

Correction factors relating the measured data to cell averaged values were generated by detailed KAPER calculations normalized to an experimental correction factor for  $^{238}\text{U}$  fission. This experimental value was achieved by comparing  $^{238}\text{U}$  fission rates measured with miniature chambers to activation results in 9C-2 and 9C-2/POS.

Table 6 contains measured data, the geometry correction factors and cell averaged fission reaction rates. A comparison to values calculated by the cell program KAPER is given. The errors quoted include calibration uncertainties and statistical errors as well as uncertainties for reproducibility and perturbation correction.

The results show that the method described in this paragraph is well suited to determine in cell fission reaction rates with sufficient accuracy. The main errors arise from the chamber calibrations itself. It should be possible to lower these errors to 1 - 1.5 % for the uranium chambers.

The comparison of experimental and calculated values (table 6) shows significant differences in the cases of  $^{238}\text{U}$ ,  $^{240}\text{Pu}$  and  $^{241}\text{Am}$ , whereas  $^{241}\text{Pu}$  fission is very well calculated. It seems necessary to extend the measurements to other isotopes like  $^{242}\text{Pu}$  and  $^{243}\text{Am}$  which are also important links in the chains of build up of high active  $\alpha$ -emitters in fast breeder reactors.

## 5. Material buckling determination

As already indicated in section 4, the material buckling can be deduced from radial and axial fission rate traverses. The basic method applied is described in /12/. From theory it follows that a detector having a cross section proportional to  $D(E) * \phi^*(E)$ , where  $D$  is the diffusion coefficient and  $\phi^*(E)$  is the adjoint flux, would give the fundamental mode of the flux distribution in a reactor. As such a detector does not exist, a "semiexperimental"  $D\phi^*$ - traverse is generated in the following manner:

The fission rate distributions of the materials  $^{235}\text{U}$ ,  $^{238}\text{U}$ ,  $^{237}\text{Np}$  and  $^{239}\text{Pu}$  are calculated, and also the  $D\phi^*$  traverse.

By comparing the calculated and experimentally determined fission rates, pointwise semiexperimental  $D\phi^*$  "rates" are then generated through a linear regression procedure.

A cosine (axially) or  $J_0$ -fit (radially) to the respective  $D\phi^+$  traverse results in the axial and radial bucklings, the sum of which gives the material buckling  $B_m^2$ .

An important modification has recently been introduced into the method. The calculation of the fission rate and  $D\phi^+$  traverses is normally done in r-z geometry. This is in good agreement with the experimental situation regarding the axial direction. Radially the situation is different. The channel for the chambers is normally not going through the core center, shim rods and unsymmetrical region borders result in azimuthally oriented perturbations of the flux giving non negligible errors of the buckling determination.

This effect is accounted for by applying correction factors to the experimental values of the fission rate distributions:

$$R_{\text{corr}} = R \frac{R_{r,z}}{R_{x,y}}$$

Here R is the measured rate and  $R_{r,z}$ ,  $R_{x,y}$  are rates calculated in r,z and x,y geometry. In the x-y calculation the actual geometry of the core is simulated as closely as possible. Thus the experimental values are transferred to an unperturbed cylindrical core directly comparable to the fission traverses calculated in r-z geometry.

Table 7 shows the buckling values of the 9C assemblies. (No buckling determination has been carried out in 9C-2/POS and 9C-2/Cu). The error of the total buckling  $B_m^2$  is about 0.3 % for 9C-1 and 9C-2, and  $\sim$  0.5 % in the other cases. The larger errors for POZ and C come from the smaller zones (only 50 central elements) in these cases, leading to a smaller area sufficiently unperturbed to give reliable results.

The theoretical results of table 7 were calculated by a zero-dimensional program of the NUSYS system, iterating to a  $k_{\text{eff}}$  equal to 1.0 minus REMO- and heterogeneity corrections.

The C/E-comparison shows a calculated overestimation by about two percent with exception of 9C-2/C, where the buckling is even underestimated. This is in contradiction to earlier experiments giving mostly theoretical overestimations of 5 % and more, using the same cross section set /12/.

## 6. Material worth measurements

### 6.1 Experiments

Material worth measurements have been performed in the critical assemblies SNEAK-9C-1 and 9C-2. A pile oscillator was used in a position 3.8 cm off the core centre. The pile oscillator cells, built of small square SNEAK platelets of 4.6 side length, were chosen to match as closely as possible the normal core compositions. As only 90 small  $\text{PuO}_2\text{UO}_2$  platelets are available at SNEAK, the pile oscillator cell in 9C-2 was diluted by an Al-platelet in order to enable a pure Pu loading over the full core height (60 cm) plus the stroke of the oscillator (80 cm). The  $^{235}\text{U}$  loading at both ends of the element remained always outside the core. Foil activation measurements showed a 2 % change in  $\sigma_{f8}/\sigma_{f5}$  in the centre of the diluted oscillator element due to the fuel reduction and the double steel sheets of the element tube. The pile oscillator cell and element configurations of SNEAK-9C-1 and 9C-2 are shown in fig. 17 and 18 respectively.

The materials investigated comprised the important fissile and fertile isotopes as well as structural and absorber materials. In 9C-2  $^{241}\text{Am}$  was measured for the first time. The samples had square or circular cross sections with 4.6 cm edge length or 4.5 cm diameter and thicknesses in the mm range. The masses were from a few grams up to 100 gr for less reactive materials.

The sample reactivities were determined by the inverse kinetic method from the flux change caused by the sample movements. Corrections for the transport of delayed neutron precursors were applied. In 9C-2 reproducibility was checked by performing two independent runs separated by a few month. Good agreement in the percent range was found.

## 6.2 Calculations

Calculations of the material worths were carried out

- with first order perturbation theory and fluxes from two dimensional diffusion calculations (DIXY). The sample materials were introduced in small quantities and homogeneous distribution in the centre of the reactor.
- with exact perturbation theory and taking into account the heterogeneity of the samples and their environment, using the KAPER code. In this case the normalization integrals were taken from diffusion calculations.

In order to convert the calculated values into dollars,  $\beta_{\text{eff}}$  values were calculated with  $\beta$  values from Keepin /19/ and using the KFKINR set.

They are

	9C-1	9C-2
$\beta_{\text{eff}}$	.00706	.00372

### 6.3 Results and conclusions

Table 8 shows experimental and calculated results of central material worths in 9C-1 and 9C-2. Here again the "central worth discrepancy", a significant overestimation of the experimental values of the fissile materials by calculation, is observed. It should be mentioned here that careful  $\beta_{\text{eff}}$  measurements carried out in the 9C cores (see chapter 9) and also in earlier SNEAK assemblies /20/, lead to the conclusion that the Keepin  $\beta$  values might be too low. Recent  $\beta$  evaluations by Tuttle /21/ result in  $\beta_{\text{eff}}$  values about 8 % higher for 9C-1 and 9C-2. With this the central worth discrepancy disappears for the fissile materials. On the other hand the underestimation of the absorber material value ( $^{10}\text{B}$ ) is even enlarged. Incorrect neutron spectrum calculations may play a role in this case.

Not clarified is the strong discrepancy of  $^{240}\text{Pu}$  in SNEAK-9C-1. Incorrect cross sections may partly be responsible, but the difference in the C/E values between 9C-1 and 9C-2 cannot be explained by this fact alone.

### 7. Reaction Rate Balance in SNEAK-9C-1 and 9C-2

The neutron balance in the centre of an assembly can serve as a check on the consistency of the reaction rates determined experimentally. All necessary experimental data for the production and loss terms are gathered in tables 4 and 8. On the production side, the  $\nu$ -value of the most abundant isotope give the greatest contribution. On the loss side, the leakage term amounts to 40 and 50 percent in 9C-1 and 9C-2, respectively. It was therefore experimentally deduced from the reactivity value of core material and the worth of a Cf neutron source.

The reactivity of core material in the core centre is given by

$$\rho_c = \frac{(DB^2\phi)\phi^+_{RL}}{\beta_{eff}\nu R_f\phi^+_f F}$$

where  $\rho_c$  is the reactivity worth of core material per  $\text{cm}^3$  in dollars,  $\phi^+_{RL}$  is the adjoint for leakage neutrons,  $DB^2\phi$  is the leakage term and  $F$  is the normalization integral. The denominator can be determined from a Cf source measurement:

$$\rho_{cf} = \frac{S_{cf}\phi^+_{cf}}{\beta_{eff}\nu R_f\phi^+_f F}$$

where  $\rho_{cf}$  is the reactivity of the source,  $S_{cf}$  is the source strength and  $\phi^+_{cf}$  is the adjoint for the source neutrons.

Combining the two equations and dividing by  $R_{f5}$  or  $R_{f9}$  in 9C-1, 9C-2, respectively, yields

$$\frac{(DB^2\phi)}{R_{fi}} = \frac{\rho_c}{\left(\frac{\rho_{cf}}{S_{cf}}\right) R_{fi}} \left(\frac{\phi^+_{cf}}{\phi^+_{RL}}\right)$$

Table 9 shows the reaction rate balances in 9C-1 and 9C-2. The errors given are  $1\sigma$  errors of the experimental values. It can be seen from the table that production and losses are in good agreement in the frame of the error limits, so that major systematical errors in the reaction rate measurements can be excluded.

8. Determination of Relative Actinide (1+α)-values

It is possible to determine (1+α)-values of fissile isotopes (α = σ<sub>c</sub>/σ<sub>f</sub>) out of fission rate and reactivity worth measurements in a critical assembly /22/.

Neglecting the scattering term, the following proportionality holds

$$\rho \sim \sigma_f (\nu \phi_f^+ - (1+\alpha) \phi_a^+) \quad (8.1)$$

where ρ is the reactivity per atom, ν is the spectrum averaged number of neutrons per fission and φ<sub>f</sub><sup>+</sup>, φ<sub>a</sub><sup>+</sup> are the adjoints of fission and absorbed neutrons respectively. The value 1+α relative to a reference isotope (index ref) is then

$$1+\alpha = \frac{\phi_f^+}{\phi_a^+} \nu - \frac{\sigma_{f,ref} \cdot \rho}{\sigma_f \cdot \rho_{ref}} * \left[ \frac{\phi_{f,ref}^+}{\phi_{a,ref}^+} \nu_{ref} - \frac{\phi_{a,ref}^+}{\phi_{a,ref}^+} (1+\alpha_{ref}) \right] \quad (8.2)$$

Measurable is the ratio

$$\frac{\sigma_{f,ref} \cdot \rho}{\sigma_f * \rho_{ref}}$$

The values for ν, φ<sup>+</sup> are calculated or taken from literature.

This method is valuable for an integral check of the capture crosssections of isotopes if no direct techniques are available. It was chosen to determine the 1+α values of a number of actinides which are important links in the build up chains for strong α-emitters in a fast reactor, e.g. the higher Pu isotopes <sup>240</sup>Pu and <sup>241</sup>Pu and <sup>241</sup>Am. The measurements analyzed in this paragraph were conducted in SNEAK-9C-2. The techniques are described in section 4.4 (fission rates) and 6 (material worths). The respective data can be found in tables 6 and 8. For reference and comparison purposes also the primary reactor materials <sup>235</sup>U, <sup>238</sup>U and <sup>239</sup>Pu were evaluated.

Before using the reactivity worth data, three corrections were applied:

- a heterogeneity correction, regarding the plate structure of the sample and its finite thickness
- a correction for the difference in composition of the pile oscillator element and the normal 9C-2 core
- a correction for the scattering contribution to the total material worth.

The heterogeneity was treated by the cell code KAPER, using KFKINR cross sections. Exact perturbation theory was used. Heterogeneous and quasihomogeneous cases were calculated, yielding the correction factors shown in table 10. No scattering data for  $^{241}\text{Am}$  were available so that no perturbation calculations could be performed for this isotope. As all corrections expressed in m $\beta$ /g have about the same magnitude, as can be seen from column two in table 10, the  $^{241}\text{Am}$  correction was taken as the average value of the other isotopes with an uncertainty of the spread of these values.

The "composition" correction was taken from 1 dim. diffusion calculations with the Karlsruhe NUSYS system and KFKINR cross sections, using first order perturbation theory. The corrections are listed in column 3 of table 10. The  $^{241}\text{Am}$  correction was taken to 1.0 with an uncertainty of the maximum correction, .04.

The scattering term was also taken from 1 dim. calculations. It was again found that it was of the same order for all isotopes and the  $^{241}\text{Am}$  value was therefore estimated from the average value. The thus corrected worths were introduced in equation (8.2). The ratios of the adjoints were calculated with KFKINR cross sections. As reference isotope  $^{239}\text{Pu}$  was chosen.

Table 11 shows the results. The errors contain only experimental uncertainties, not those of  $\nu$  or the calculated adjoint values. The comparison with calculated  $(1+\alpha)$  values shows good agreement for  $^{235}\text{U}$ ,  $^{238}\text{U}$  and  $^{241}\text{Pu}$ . There is also a very good agreement found for  $^{238}\text{U}$  between the method described in this paragraph and activation results (see section 4.3.2). Poor agreement is found for  $^{240}\text{Pu}$ . Here capture is significantly underestimated by calculation. A strong discrepancy exists also for  $^{241}\text{Am}$ , where a factor of 2 is found between experiment and calculation. This shows that cross sectional data may be highly uncertain for the non primary actinides including those not investigated in this work, e.g.  $^{242}\text{Pu}$ ,  $^{243}\text{Am}$ .

## 9. Measurements of $\beta_{\text{eff}}$ in SNEAK-9C-1 and 9C-2

In the pursuit of a program which was initiated on earlier SNEAK assemblies, experiments to determine  $\beta_{\text{eff}}$  by the  $^{252}\text{Cf}$  technique were performed in the assemblies 9C1 and 9C2. As this program is described in a separate publication, /20/ the measurements will only be briefly outlined in this report.

### 9.1 Measurement with a calibrated $^{252}\text{Cf}$ Source

The method consists of measuring the central worth of a  $^{252}\text{Cf}$  source, and the absolute fission rate. As shown in /20/, these measurements give essentially the product  $\beta_{\text{eff}} \bar{\nu} F$ , where  $\bar{\nu}$  is the average number of fission neutrons per fission, and  $F$  is the normalization integral. Experimental values for the normalization integral were deduced from fission chamber traverses along the main axes of the cores and from importance traverses measured with the  $^{252}\text{Cf}$  source.

The axial importance traverse in 9C2 is shown in Fig. 19. Then, using  $\bar{\nu}$  as calculated from basic data, one obtains experimental values for the  $\beta_{\text{eff}}$ .

The results of the central  $^{252}\text{Cf}$  worth and fission rate measurements are given in Table 12. The  $^{252}\text{Cf}$  worth in 9C1 was measured in the radial, and in the axial channel. The  $^{252}\text{Cf}$  worth in 9C-2 has a slightly larger error, due to an additional uncertainty in the calibration of the automatic control rod. The fission rate refers to  $1 \text{ cm}^3$  of core composition at the core center.

The two slightly different values for the fission rate in 9C2 refer to different assessments of the fissile deposit in the  $^{239}\text{Pu}$  fission chamber. The value used in /20/ is based on a calibration effort by  $\alpha$  counting, published by Pinter et al. /14/, and corresponds to a deposit of 29.038  $\mu\text{g}$ . However, recent precision measurements of the half-life of  $^{239}\text{Pu}$  by Oetting/16/, and by Aleksandrov /17/ lead us to adopt the value of 28.665  $\mu\text{g}$ , which is used throughout this report. Though the difference is only 1.3 %, and therefore not really significant, both results are quoted, to avoid confusion with other publications.

The experimental  $\beta_{\text{eff}}$ ,  $\nu F$ , normalization integrals, and  $\beta_{\text{eff}}$  are shown in Table 13. To obtain the calculated  $\beta_{\text{eff}}$  values, the  $\beta$ -values by Keepin /19/ (delayed neutrons per fission divided by  $\bar{\nu}$  for the fission spectrum) were used. The  $\beta_{\text{eff}}$  are underestimated by 7 % in 9C1, and 12 % in 9C2.

## 9.2 Measurements of $\beta_{\text{eff}}$ Ratios by the Pile Oscillator Technique

In 9C2, a different experimental technique was also used. It consisted of measuring, in a pile oscillator experiment, the apparent reactivity due to the transport of delayed neutron precursors out of the core. Four different loadings of the pile oscillator subassembly were used, in order to measure the effect of precursors of different isotopes. The reference loading, Pu1, had essentially the core composition, containing the heavy isotopes  $^{239}\text{Pu}$  and  $^{238}\text{U}$ . In the loading U1, Pu was replaced by  $^{235}\text{U}$ . Pu2 and U2 had the same fissile content as Pu1 and U1, but inert material was replaced by additional  $^{238}\text{U}$ . These experiments give ratios of delayed neutron yields  $\nu_d$  for the isotopes  $^{235}\text{U}$ ,  $^{238}\text{U}$  and  $^{239}\text{Pu}$  with good accuracy.

## 9.3 Results and Conclusions

The results of all the  $\beta_{\text{eff}}$  experiments are summarized in Table 14. For comparison, calculated values using the delayed neutron yields from Keepin /19/, and from a recent evaluation by Tuttle /21/ are also given.

Both the  $\beta_{\text{eff}}$  and the ratio are underestimated with the Keepin data. The prediction of the  $\beta_{\text{eff}}$  is slightly improved if one divides delayed neutron yields per fission by  $\bar{\nu}$  for the core spectrum, rather than for the fission spectrum. However, if the Tuttle data are used, the deviations are at most slightly larger than the error limits. Therefore these experiments confirm, in general, the Tuttle evaluation, except that they indicate a slightly higher  $^{239}\text{Pu}$  yield.

References

- /1/ R. Böhme, F. Helm, S. Pilate, M. Pinter, W. Scholtyssek  
Critical Experiments at SNEAK in Support of Fast Reactor  
Design  
ANS Topical Meeting on Advanced Reactor Physics, Design  
and Economics, Atlanta, September 1974
- /2/ M. Pinter et al.  
Physics Investigations of Sodium Cooled Fast Reactors;  
SNEAK Assembly 9A  
KFK 2028 (1974)
- /3/ M. Pinter et al.  
Control Rod Worth and Power Distribution Measurements in  
the SNR Mock Up SNEAK Assembly 9A  
KFK 2077 (1974)
- /4/ G. Jourdan et al.  
Physics Investigations of Sodium Cooled Fast Reactors;  
SNEAK Assembly 9B  
KFK 2012 (1974)
- /5/ F. Helm et al.  
Physics Investigations of Sodium Cooled Fast Reactors;  
SNEAK Assembly 2  
KFK 1399 (1971)
- /6/ W. Hoebel  
"DIXY", Unpublished Computer Program,  
GfK Karlsruhe
- /7/ E. Kiefhaber  
The KFKINR-set of Group Constants; Nuclear Data Basis  
and First Results of its Application to the Recalculation  
of Fast ZERO-Power Reactors  
KFK 1572 (1972)
- /8/ C. Günther, W. Kinnebrock  
Das eindimensionale Transportprogramm DTK  
KFK 1381 (März 1971)

- /9/ C. Günther, W. Kinnebrock  
SNOW, Ein zweidimensionales  $S_N$ -Programm zur Lösung der  
Neutronentransportgleichung in Platten- und Zylinder  
Geometrie  
KFK 1826, Juli 1973
- /10/ H. Huschke  
Gruppenkonstanten für dampf- und natriumgekühlte schnelle  
Reaktoren in einer 26-Gruppendarstellung  
KFK 770 (1968)
- /11/ P.E. McGrath  
KAPER - Lattice Program for Heterogeneous Critical Facilities  
KFK 1893 (1973)
- /12/ H. Küsters  
Progress in Fast Reactor Physics in the Federal Republic  
of Germany  
KFK 1632 (1973)
- /13/ R. Böhme  
Messung des Einflusses von Kontrollstäben auf die Leistungs-  
verteilung in der SNR300 Nachbildung SNEAK 9A-2  
- Spaltkammertraversen -  
PSB-Vierteljahresbericht 1/1973 (pp. 121-15)  
KFK 1273/1 (1973)
- /14/ M. Pinter et al.  
Interlaboratory Comparison of Absolute Fission Rate and  
Uranium 238 Capture Rate Measurements in the MOL  $\Sigma\Sigma$   
Secondary Intermediate Energy Standard Neutron Field.  
Conference on Nuclear Cross Sections and Technology  
Washington D.C., March 3-7, 1975
- /15/ D. Gilliam, NBS,  
Washington D.C., priv. not.

- /16/ F.L. Oetting, R.F.P.-1469 (1971)
- /17/ B.M. Aleksandrov et al.  
The Halflife of  $^{239}\text{Pu}$   
Bulletin of the Academy of Sciences of the USSR. Physical  
Series 39/3 pp 20-25 (1975)
- /18/ E.A. Fischer et al.  
Physics Investigations of two Pu-Fueled Fast Critical  
Assemblies: SNEAK 7A and 7B  
KFK 1939 (March 1974)
- /19/ G.R. Keepin  
Physics of Nuclear Kinetics  
Addison Wesley, New York (1965)
- /20/ E.A. Fischer  
Integral Measurements of the Effective Delayed Neutron  
Fractions in the Fast Critical Assembly SNEAK  
(To be published in Nucl. Sci. Eng.)
- /21/ R.J. Tuttle  
Delayed Neutron Data for Reactor Physics Analysis  
Nucl. Sci. Eng. 56, 37, (1975)
- /22/ F. Feiner, L.J. Esch  
Reactor Physics in the Resonance and Thermal Regions  
Vol. II, 1966, The MIT Press, Cambridge, USA

List of tables

table 1	Particle densities of 9C core compositions
table 2	Evaluation of Critical Experiments
table 3	Characteristic data of SNEAK standard fission chambers
table 4	Cell averaged fission and capture reaction rates in SNEAK 9C
table 5	Characteristic data of SNEAK miniature chambers
table 6	Experimental and calculated fission rate ratios of higher actinides in SNEAK-9C
table 7	Material buckling determination in the SNEAK-9C assemblies
table 8	Central material worths in SNEAK 9C1 and 9C2
table 9	Reaction rate balances in SNEAK 9C1 and 9C2
table 10	Correction of reactivity values in SNEAK 9C2
table 11	Actinide reaction rate ratios in 9C-2 and evaluated $(1+\alpha)$ values
table 12	Results of the Central $^{252}\text{Cf}$ Worth, and Fission Rate Measurements
table 13	Results of $\beta_{\text{eff}}$ Measurements with a $^{252}\text{Cf}$ Source
table 14	Experimental Results and Comparison with Evaluated Delayed Neutron Yields

List of figures

- Fig. 1            a) Cross section of 9C-1  
                  b) r-z-diagram of 9C-1
- Fig. 2            Core cells of 9C-1
- Fig. 3            a) Cross section of 9C-2  
                  b) r-z-diagram of 9C-2
- Fig. 4            Core cells of 9C-2
- Fig. 5            Cross sections of central substitution zones  
                  in 9C2
- Fig. 6            r-z-diagrams of central substitution zones  
                  in 9C2
- Fig. 7a           Unit cells of central substitution zones POS,  
                  POZ and C zone
- Fig. 7b,c        Cells for axial and radial channels in SNEAK  
                  9C2/POZ and 9C2/C
- Fig. 8a-d        Axial reaction rate traverses of  $^{235}\text{U}$ ,  $^{238}\text{U}$ ,  
                   $^{239}\text{Pu}$  in 9C2
- Fig. 9a-d        Radial reaction rate traverses of  $^{235}\text{U}$ ,  $^{238}\text{U}$ ,  
                   $^{239}\text{Pu}$  in 9C2
- Fig. 10          Cell for fine structure measurement in 9C2/POZ
- Fig. 11           $^{238}\text{U}$  fission and  $^{238}\text{U}$  capture fine structure  
                  in the 9C1 cell

- Fig. 12       $^{238}\text{U}$  reaction rate fine structures in the 9C2 cell
- Fig. 13       $^{238}\text{U}$  reaction rate fine structures in 9C2/POS
- Fig. 14a,b     $^{238}\text{U}$  reaction rate fine structures in 9C2/POZ
- Fig. 15       $^{238}\text{U}$  reaction rate fine structure in 9C2/C
- Fig. 16      Experimental arrangement of in cell measurements with miniature fission chambers
- Fig. 17      Oszillator cell and element configuration in SNEAK 9C1
- Fig. 18      Oszillator cell and element configuration in SNEAK 9C2
- Fig. 19      Axial importance traverse in SNEAK 9C2

Table 1 Particle densities of SNEAK 9C compositions  
atomic densities /  $10^{24} \text{ cm}^{-3}$

	SNEAK 9C-1		9C-2		POS		POZ			C-zone			Blanket	Control rod
	M1	M2	M3	M4	M5	M6	M7	M8	M9	M10	M11	M12	MB	MK
Al	-	.3836-3	.603-5	.4387-3	-	.41796-3	.50143-5	.50668-5	.4928-3	.10816-5	.11375-5	.50997-3	-	.3560-2
C	.3089-2	.3152-2	.497-4	.4916-3	.3361-4	.47037-3	.66347-4	.63186-4	.5468-3	.92339-2	.92311-2	.56434-3	.136-4	.3679-2
Ca	-	-	.568-5	.499-5	-	.50226-5	.69633-6	-	.4903-5	.95219-6	-	.48756-5	-	-
Cr-Mn	.2850-2	.2685-2	.3031-2	.3048-2	.30171-2	.30471-2	.3055-2	.30551-2	.30501-2	.36796-2	.36798-2	.30508-2	.12-2	.3173-2
Cu	-	-	-	-	-	-	.65688-3	.6562-3	-	.69782-3	.69713-3	-	-	-
Ga +)	-	-	-	-	-	-	.14104-3	.1412-3	-	.14983-3	.15001-3	-	-	-
Fe	.1124-1	.1119-1	.1030-1	.1036-1	.1031-1	.10359-1	.1232-1	.1232-1	.1037-1	.12318-1	.12318-1	.10372-1	.3955-2	.10802-1
H	.2377-4	.2408-4	-	.325-5	-	.30922-5	.14894-4	.16294-4	.3654-5	.10394-4	.11882-4	.37829-5	-	.2668-4
K	.250-5	.254-5	-	.353-6	-	.336-6	-	-	.397-6	-	-	.41105-6	-	.290-5
Mg	-	.393-5	.268-5	.679-5	-	.65929-5	.17725-5	.17725-5	.73044-5	-	-	.74675-5	-	.365-4
Mo	.123-4	.110-4	.219-4	.192-4	.17047-4	.19339-4	.19499-4	.19499-4	.18878-4	.26805-4	.26806-4	.18772-4	.997-5	-
Na	.8865-2	.8686-2	.8328-2	.8192-2	.83210-2	.81981-2	.73684-2	.73684-2	.81746-2	.78276-2	.7828-2	.81692-2	-	.7210-2
Nb	.854-5	.762-5	.879-5	.772-5	.85439-5	.77709-5	.87047-5	.87047-5	.75858-5	.8544-5	.8544-5	.75433-5	.854-5	-
Ni	.2327-2	.2255-2	.1665-2	.1665-2	.20026-2	.16646-2	.26576-2	.26582-2	.16645-2	.20199-2	.20207-2	.16645-2	.9845-3	.1659-2
∅	.1231-1	.1216-1	.1636-1	.1570-1	.16266-1	.15731-1	.1578-1	.15776-1	.15616-1	.39802-5	.14495-6	.1559-1	-	.10905-1
Pu-239	-	-	.1975-2	.1735-2	.17209-2	.17465-2	.17689-2	.17818-2	.17049-2	.18791-2	.189297-2	.16954-2	-	-
Pu-240	-	-	.1775-3	.1559-3	.45424-3	.1569-3	.42883-3	.42298-3	.15316-3	.45556-3	.44937-3	.1523-3	-	-
Pu-241 <sup>+++)</sup>	-	-	.1026-4	.9010-5	.1344-3	.90709-5	.6296-4	.6075-4	.88549-5	.6688-4	.6454-4	.88053-5	-	-
Pu-242	-	-	.813-6	.714-6	.3840-4	.71873-6	.14036-4	.11003-4	.70161-6	.14913-4	.1169-4	.69768-6	-	-
Si	.1215-3	.1249-3	.1388-3	.1405-3	.14053-3	.14045-3	.14312-3	.14345-3	.14074-3	.16833-3	.16869-3	.1408-3	.453-4	.1527-3
Ta	-	-	.135-6	.118-6	-	.1193-6	-	-	.11644-6	-	-	.11579-6	-	-
Ti	.119-4	.148-4	-	.472-5	-	.44967-5	.20566-6	.20594-6	.53137-5	.21225-4	.21226-4	.55012-5	-	.388-4
U-235	.3078-2	.3071-2	.4390-4	.4052-3	.4481-4	.38784-3	.41471-4	.41471-4	.45034-3	.43793-4	.43796-4	.46467-3	.1625-3	.30116-2
U-236	-	-	.271-6	.238-6	-	.23969-6	-	-	.23398-6	-	-	.23267-6	-	-
U-238	.7108-2	.7085-2	.5963-2	.6076-2	.57593-2	.60705-2	.57179-2	.57179-2	.60902-2	.70451-2	.70455-2	.60946-2	.3994-1	.6894-2
B 10 <sup>+++)</sup>	-	-	.828-5	.727-5	.83254-5	.73213-5	-	-	.71466-5	-	-	.71069-5	-	-

+++)  
+) in replacement of gold ( $N_{B10} = 1/3 \times N_{Au}$ )  
+) was added to copper in calculations  
++) valid for 1.9.1974

Table 2 Critical Experiment Evaluations of SNEAK 9C assemblies

Assembly	9C-1	9C-2	9C-2/POS	9C-2/POZ	9C-2/C
2-dim. r-z-diffusion	1.0048	1.0018	1.0013	.9931	.9909
Transport { axial 1-dim. { radial	.0035 .0058	.0046 .0078	.0046 .0077	.0043 .0075	.0048 .0079
Heterogeneity	.0005	-.0010	-.0014	.0044	.0039
REMO	-.0016	.0002	.0001	.0002	.0003
Cylindrization	-.0020	-.0040	-.0036	-.0035	-.0025
CHi	.0002	-.0010	-.0010	-.0009	-.0008
Calculation	1.0112	1.0084	1.0077	1.0051	1.0045
Experiment	1.0007	1.0004	1.0001	1.0001	1.0010
C/E	1.0105	1.0080	1.0076	1.0050	1.0035

Table 3 Characteristic data of SNEAK standard fission chambers used in 9C irradiation experiments

chamber identification	main isotope	total fissile mass / $\mu\text{gr}$ (error* / %)	isotopic composition (weight %)	geometry
Unat-20	$^{238}\text{U}$ (natural Uranium)	325 (1.5)	$^{234}\text{U}$ .0055 $^{235}\text{U}$ .7115 $^{238}\text{U}$ 99.283	chamber diameter: 26 mm height: 20 mm  gas filling: argon-methane pressure: 1.2 atm  applied voltage: $\sim$ 180 V  diameter of active layer: 15 mm
U5-22	$^{235}\text{U}$	311 (1.6)	$^{234}\text{U}$ .57 $^{235}\text{U}$ 95.27 $^{238}\text{U}$ 4.16	
Pu9-25	$^{239}\text{Pu}$	28.665 (0.8)	$^{239}\text{Pu}$ 96.04 $^{240}\text{Pu}$ 3.75 $^{241}\text{Pu}$ .12	

\*  $2\sigma$ -statistical error

+ sum of systematic errors

Table 4 Cell averaged fission and capture reaction rates in SNEAK 9C

		cross section ratio in center of assembly (1 $\sigma$ error / %)						
		9C-1	9C-2	9C-2/POS	9C-2/POZ	9C-2/C	9C-2/Cu	
Experiment	$\sigma_{f8}/\sigma_{f5}$	.04754 (1.5)	.04633 (1.2)	.04615 (1.3)	.04311 (1.5)	.04445 (1.5)	.04508 (1.3)	*)
	$\sigma_{f9}/\sigma_{f5}$	1.155 (3.0)	1.104 (1.5)	1.097 (1.7)	1.084 (1.7)	1.114 (1.5)	1.117 (1.7)	*)
	$\sigma_{c8}/\sigma_{f5}$	.1292 (2.2)	.1313 (2.2)	.1272 (2.5)	.1330 (2.5)	.1333 (2.5)	.1270 (2.5)	**)
C/E	$\frac{\sigma_{f8}}{\sigma_{f5}}$ KAPER	.9062	.9007	.8947	.8794	.9154	.9166	
	$\frac{\sigma_{f8}}{\sigma_{f5}}$ DIFF	.8992	.8988	.8841	.9061	.9372	.9013	
	$\frac{\sigma_{f9}}{\sigma_{f5}}$ KAPER	.9405	.9363	.9417	.9556	.9592	.9245	
	$\frac{\sigma_{f9}}{\sigma_{f5}}$ DIFF	.9416	.9353	.9418	.9475	.9472	.9241	
	$\frac{\sigma_{c8}}{\sigma_{f5}}$ KAPER	.9799	1.0008	1.0369	.9902	.9640	1.0354	
	$\frac{\sigma_{c8}}{\sigma_{f5}}$ DIFF	.9845	1.0015	1.0369	1.0000	.9715	1.0378	

an additional error of 0.5 % (\*\*) should be taken into account for reproducibility  
 1.0 % (\*\*)

Table 5 Data of SNEAK miniature fission chambers

chamber No.	main isotope	total mass of <u>fissile material</u> μgr (1σ error/%)		isotopic vector at %					
				<sup>234</sup> U	<sup>235</sup> U	<sup>238</sup> U	<sup>239</sup> Pu	<sup>240</sup> Pu	<sup>241</sup> Pu
1722-1	<sup>238</sup> U	222.	(2.0)	.0055	.7203	99.2742			
1722-2		253.	(2.0)						
1724-1	<sup>235</sup> U	58.7	(2.0)	.17	99.5	.30			
1724-2		41.9	(2.0)						
1725-2	<sup>239</sup> Pu	21.5	(0.7)	96.09	3.74	.12	.01	.07	
1725-3		29.76	(0.7)						
1726-4-8	<sup>240</sup> Pu	76.0	(1.3)	.78	98.46	.16	.17	.43	
1727-3-8	<sup>241</sup> Pu	31.8	(1.5)	*) 1.05	3.66	88.92	1.85	4.52	
Am241-8-3	<sup>241</sup> Am	5.251	(1.4)					100.	

\*) valid for 4.6.74

Table 6 Experimental and calculated fission rate ratios  
of higher actinides in SNEAK-9C

Isotope	$\sigma_f/\sigma_f(^{235}\text{U})$		$\frac{1\sigma \text{ error}}{\%}$	cell average chamber posit. (calculated)	$\sigma_f/\sigma_f(^{235}\text{U})$		$\frac{1\sigma \text{ error}}{\%}$	*) C/E	
	(chamber position)				(cell averaged)			9C-2	9C-2/POS
	9C-2	9C-2/POS			9C-2	9C-2/POS		9C-2	9C-2/POS
$^{238}\text{U}$	.04455	.04467	2.3	1.037 ± .011 <sup>**)</sup>	.04620	.04632	2.5	.907	.898
$^{239}\text{Pu}$	1.088	1.095	2.7	1.006 ± .006	1.094	1.101	2.8	.945	.939
$^{240}\text{Pu}$	.3203	.3235	3.0	1.025 ± .009	.3283	.3316	3.2	.902	.887
$^{241}\text{Pu}$	1.322	1.337	3.0	1.001 ± .006	1.323	1.338	3.1	1.001	.990
$^{241}\text{Am}$	.2783	.2796	3.1	1.023 ± .009	.2847	.2856	3.2	1.337	1.327

\*) calculations by KAPER and KFKINR cross sections

\*\*\*) the  $^{238}\text{U}$  correction was achieved by comparing miniature chamber results to foil measurements

Table 7 Material buckling determination in the SNEAK-9C assemblies

Assembly	$B_m^2/m^{-2}$			Calculation (KFKINR-set) total	C/E
	Experiment axial	radial	total		
9C-1	12.00 ±.03	19.73 ±.04	31.73 ±.05	32.57	1.026
9C-2	11.63 ±.05	20.30 ±.05	31.93 ±.07	32.50	1.018
9C-2/POZ	11.49 ±.04	20.54 ±.05	32.03 ±.06	32.72	1.022
9C-2/C	11.89 ±.04	20.67 ±.09	32.56 ±.10	32.30	.992

Table 8 Material worths at the Core Centre,  $10^{-3}$   $\beta$ /g

Sample	Sample weight g	SNEAK-9C-1 ( $\beta_{\text{eff}} = .00706$ )				SNEAK-9C-2 ( $\beta_{\text{eff}} = .00372$ )			
		Experiment (1 $\sigma$ error/%)	KAPER (het)	Diffusion (hom)	$C_{\text{het}}/E$	Experiment (1 $\sigma$ error/%)	KAPER (het)	Diffusion (hom)	$C_{\text{het}}/E$
$^{235}\text{U}$	6.69	.471 (2)	.493	.491	1.04	1.112 (2)	1.215	1.259	1.09
$^{238}\text{U}$	123.6	- .0241 (5)	- .027	- .021	1.12	- .050 (5)	- .0625	- .0609	1.24
$^{239}\text{Pu}$	4.04	.766 (4)	.817	.789	1.07	1.67 (2)	1.79	1.822	1.07
$^{240}\text{Pu}$	2.7	.144 (4)	.226	.224	1.57	.336 (6)	.432	.447	1.32
$^{241}\text{Pu}$	1.16	.962 (5)	.966	.942	1.004	2.006 (4)	2.26	2.326	1.13
$^{241}\text{Am}$	3.535	--	--	--	--	- .119 (10)	--	--	--
$^{10}\text{B}$	.589	- 11.1 (5)	- 10.9	- 10.5	.98	- 22.5 (4)	- 21.7	- 24.44	.96
Stainless Steel	54.7	- .015 (5)	- .014	- .012	.93	- .052 (5)	- .048	- .052	.93
Na	9.97	+ .011 (5)	--	.026	--	- .059 (5)	- .044	- .053	.75
Cu	59.51	--	--	--	--	- .087	- .093	--	1.07
Cf-Source (1/ $\beta_{\text{eff}}$ ) ( $10^3\beta/\text{cm}^3$ )	--	.508 (4)	.554	--	1.09	.784 (4)	.900	--	1.15
Corematerial ( $10^3\beta/\text{cm}^3$ )	direct cell measurement synthesized value	.531 .522				1.13 1.121			

Table 9 Reaction rate balances in SNEAK-9C-1 and 9C-2

	9C-1		9C-2	
	(1σ error)		(1σ error)	
Production	$v_5$	2.488	$v_9$	2.977
	$v_8 R_{f8}/R_{f5}$	.307 (.003)	$v_8 R_{f8}/R_{f9}$	.360 (.006)
		<u>2.795</u> ( <u>.003</u> )	$v_5 R_{f5}/R_{f9}$	.050 (.001)
			$(v_{40} R_{f40} + v_{41} R_{f41})/R_{f9}$	.106 (.002)
				<u>3.493</u> ( <u>.007</u> )
Losses	$1+\alpha_5$	1.218	$1+\alpha_9$	1.173
	$R_{f8}/R_{f5}$	.109 (.001)	$R_{f8}/R_{f9}$	.127 (.002)
	$R_{c8}/R_{f5}$	.298 (.006)	$R_{c8}/R_{f9}$	.357 (.010)
	$R_{cst}^*/R_{f5}$	.043	$R_{a5}/R_{f9}$	.025
	$-R_{n,2n}/R_{f5}$	- .007	$(R_{a40}/R_{a41})/R_{f9}$	.049
	$(DB^2\phi)/R_{f5}$	1.132 (.029)	$R_{cst}^*/R_{f9}$	.066
		<u>2.793</u> ( <u>.030</u> )	$-R_{n,2n}/R_{f9}$	- .008
		$(DB^2\phi)/R_{f9}$	1.749 (.065)	
			<u>3.538</u> ( <u>.070</u> )	
Production				
- Losses		.002 (.030)		- .045 (.070)

\* capture in materials not listed in the table (calculated)

Table 10 Correction of reactivity values in 9C-2

	$\rho_{\text{measured}}$ (m\$g/g) (1 $\sigma$ error/%)	Heterogeneity correction Hom-Het (m\$g/g)	"Composition" correction clean 9C-2/ Pile oscillator	Scattering contribution (m\$g/g)	$\rho_{\text{corrected}}$ (m\$g/g) (1 $\sigma$ error/%)
<sup>235</sup> U	1.11 (2)	- .014	1.022	- .0145	1.137 (2.5)
<sup>238</sup> U	- .050 (5)	- .009	.965	- .0172	- .040 (10)
<sup>239</sup> Pu	1.67 (2)	- .020	1.024	- .0110	1.701 (2.5)
<sup>240</sup> Pu	.336 (6)	- .010	1.038	- .0136	.352 (7)
<sup>241</sup> Pu	2.01 (4)	- .010	1.021	- .0082	2.050 (4)
<sup>241</sup> Am*	- .119 (10)	- .014 ±.007	1.000 (.04)	-(.0129 ±.005)	- .120 (18)

\* the correction terms for <sup>241</sup>Am were determined from the calculated ones for the other isotopes

Table 11 Actinide reaction rate ratios in 9C-2 and  
evaluated (1+α) values (1σ error in %)

	$^{235}\text{U}$	$^{238}\text{U}$	$^{239}\text{Pu}$	$^{240}\text{Pu}$	$^{241}\text{Pu}$	$^{241}\text{Am}$
1) $\rho/\rho(^{239}\text{Pu})$	.657 (3.5)	- .023 (10)		.208 (7.5)	1.215 (5)	- .071 (18)
$\sigma_f/\sigma_f(^{239}\text{Pu})$	.914 (2.8)	.0422 (2.8)		.300 (1.5)	1.209 (1.5)	.26 (1.8)
$\nu$ 2)	2.485	2.842	2.978	3.172	2.979	3.327
1+α Exper.	1.20 (4.5)	3.99 (4.0)		1.94 (5.0)	1.16 (8)	3.97 (2.5)
Calc.	1.24	4.22	1.173 <sup>3)</sup>	1.56	1.18	2.03
Activation experiment <sup>4)</sup>		3.83 (2.2)				

1) Reactivity per atom, scattering term subtracted

2) from KFKINR cross sections

3) reference value for experimental evaluation

4) see table 4

Table 12 Results of the Central  $^{252}\text{Cf}$  Worth, and Fission Rate Measurements

	$^{252}\text{Cf}$ source strength $10^6$ n/sec	$\rho_{\text{Cf}}$ , m%	Current of $\text{BF}_3$ chamber, $10^{-8}$ Amp.	$\frac{\rho_{\text{Cf}}}{S_{\text{Cf}}}$ J $10^{-16}$ g-A	Calculated adjoint ratio $\phi_{\text{Cf}}^+/\phi_f^+$	Fission Rate <sup>c)</sup>
9C1 <sup>a)</sup>	0.496±2 %	10.07±3 %	0.1237	0.251		
9C1 <sup>b)</sup>	0.485±2 %	8.87±3 %	0.1340	0.245		
Average				0.248±2.5 %	1.010	20.66±1.5 %
9C2	0.460±2 %	15.14±3.5 %	0.1306	0.430±4 %	1.009	18.14±1.5 % <sup>d)</sup> (18.37±1.5 %) <sup>e)</sup>

a) in the radial channel

b) in the axial channel

c) in  $10^{12}$  fissions/( $\text{cm}^3$ -sec-Amp. of chamber current)

d) based on a Pu deposit of 29.038  $\mu\text{g}$  /14/

e) based on a Pu deposit of 28.665  $\mu\text{g}$

Table 13 Results of  $\beta_{\text{eff}}$  Measurements with a  $^{252}\text{Cf}$  Source

Assembly	Experiment		Calculation (KFK/INR)			$\beta_{\text{eff}}$ deduced from Experiment
	$\beta_{\text{eff}}$	$\bar{\nu} F^{\text{a)}$	$F$	$\beta_{\text{eff}}$	$\bar{\nu}$	
9C2	1293±4.3%	102520±1.5%	.00372	2.96	100870	.00426±4.5% <sup>b)</sup>
	1279±4.3%	102520±1.5%				.00421±4.5% <sup>c)</sup>
9C1	1969±2.9%	103020±1.5%	.00706	2.52	101580	.00758±3.2%

$$\text{a) } \beta_{\text{eff}} \bar{\nu} F = \left( \frac{S_{\text{cf}}}{\rho_{\text{cf}} \cdot J} \right) \left( \frac{\phi_{\text{cf}}^+}{\phi_f^+} \right) / (R_f/J)$$

b) based on  $m_g = 29.038 \mu\text{g}$

c) based on  $m_g > 28.665 \mu\text{g}$

Table 14 Experimental Results and Comparison with Evaluated Delayed Neutron Yields

SNEAK assembly	$\beta_{\text{eff}}$		Pile Oscillator Measurements	
	9C1	9C2 <sup>c)</sup>	$\nu_{\text{d8}}/\nu_{\text{d5}}$	$\nu_{\text{d9}}/\nu_{\text{d5}}$ <sup>c)</sup>
<u>Experiment</u>	.00758	.00421	2.66±3%	0.399±3%
<u>Calculation</u>				
Data from Keepin <sup>a)</sup>	.00706	.00372		
Data from Keepin <sup>b)</sup>	.00722	.00379	2.50	0.382
Data from Tuttle <sup>b)</sup>	.00754	.00404	2.656	0.386

a) delayed neutrons per fission, divided by  $\bar{\nu}$  for the fission spectrum

b) delayed neutrons per fission, divided by  $\bar{\nu}$  for the core spectrum

c) based on  $m_{\text{fiss}} = 28.665 \mu\text{g}$

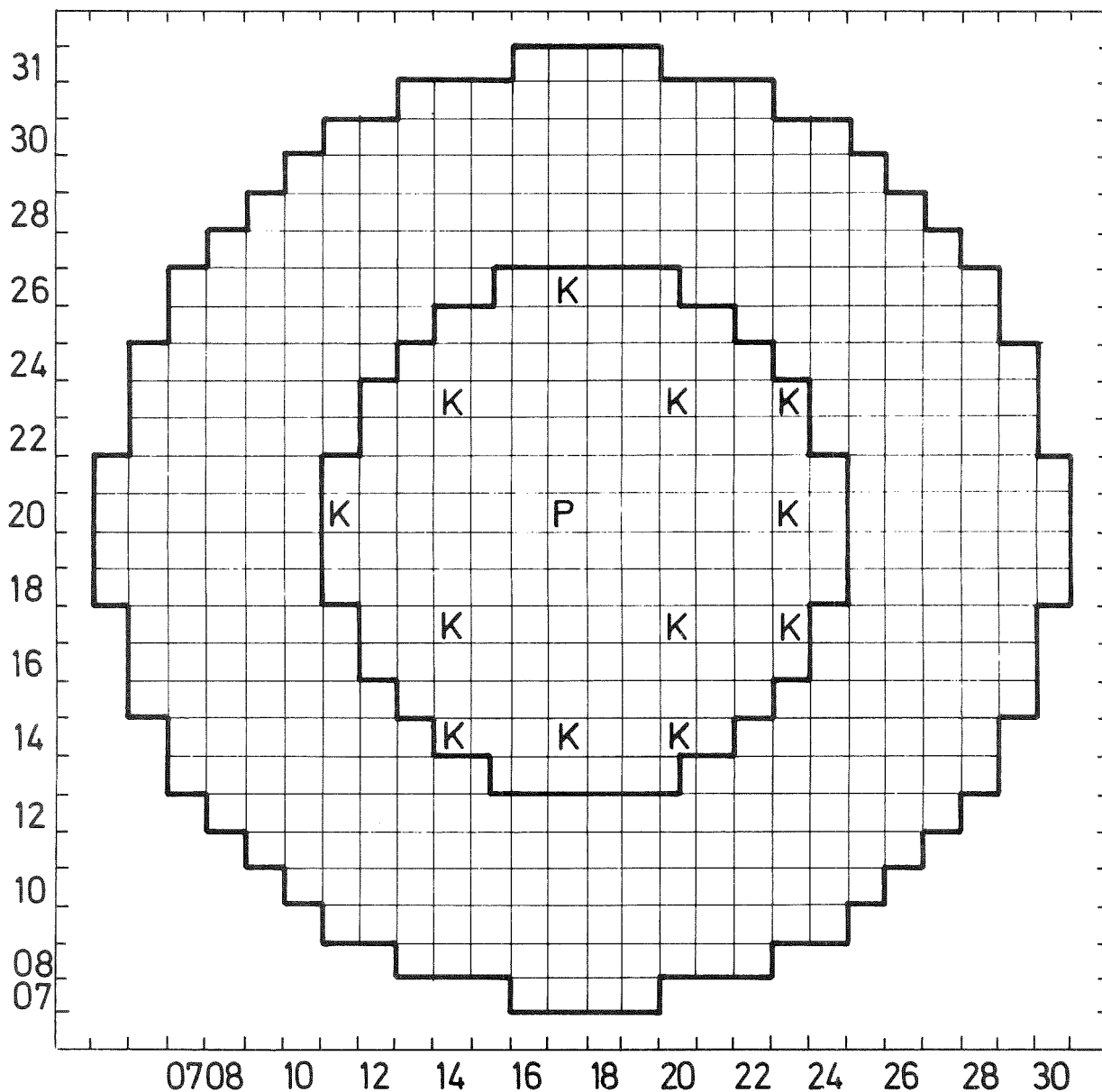
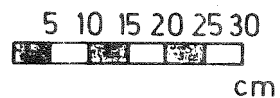
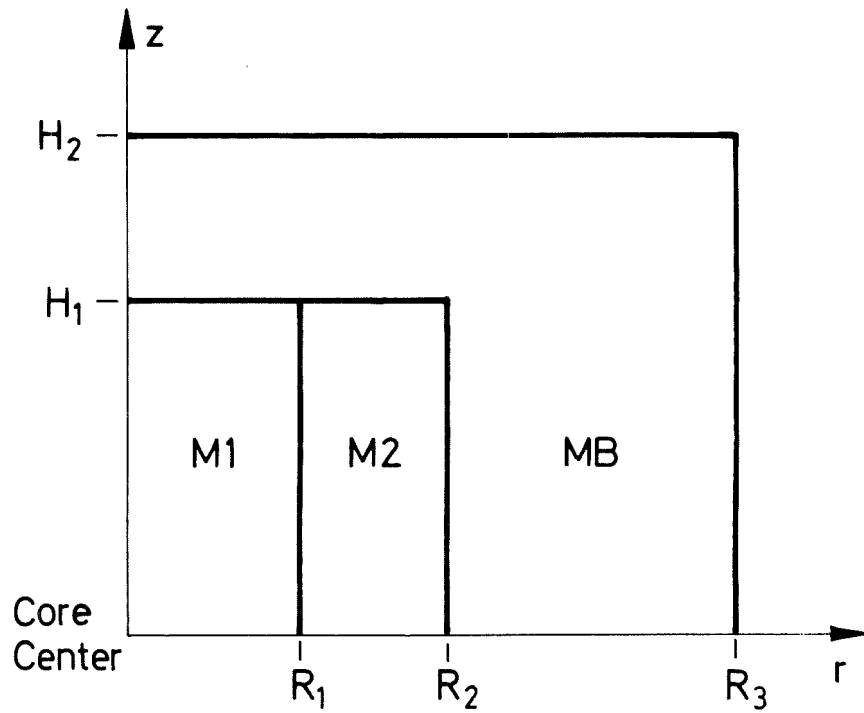


Fig. 1a Crosssection of SNEAK 9C -1  
critical experiment

- K SNEAK control rod
- P Position for pile oscillator



$$R_1 = 19.41 \text{ cm} \qquad H_1 = 29.98 \text{ cm}$$

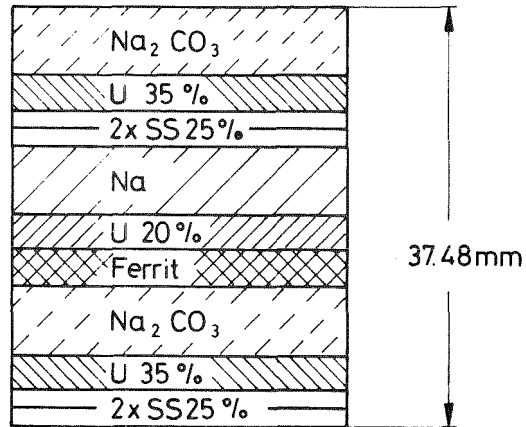
$$R_2 = 37.59 \text{ cm} \qquad H_2 = 60.46 \text{ cm}$$

$$R_3 = 68.63 \text{ cm}$$

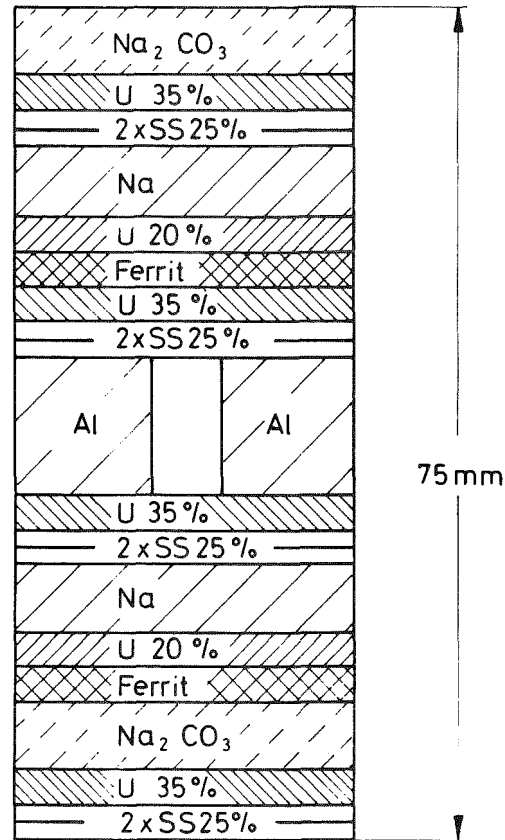
$M_i$  Mixture number of regions with constant particle densities

Fig.1b Geometrical model for the  $r$ - $z$  diffusion calculation

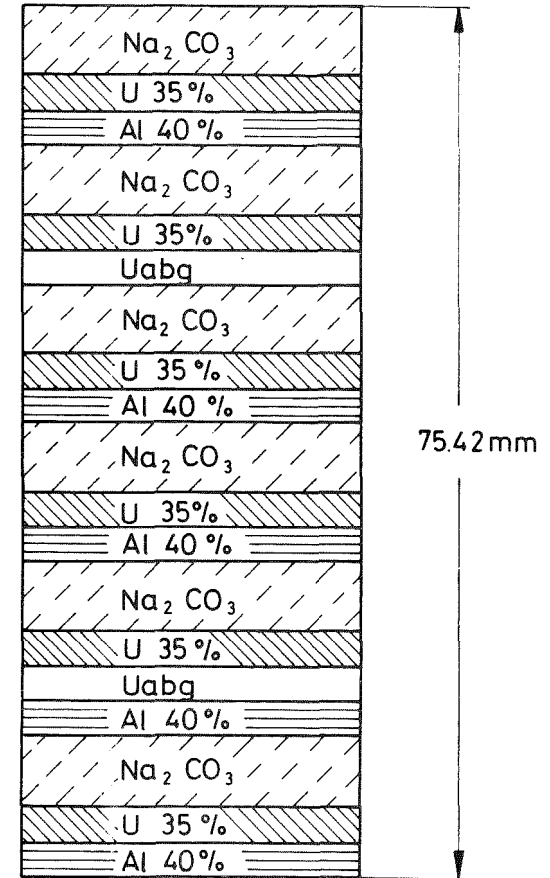
Fig. 2a Core cells used in SNEAK 9C-1



Normal cell



Window cell for the channel



Unit cell for control rod

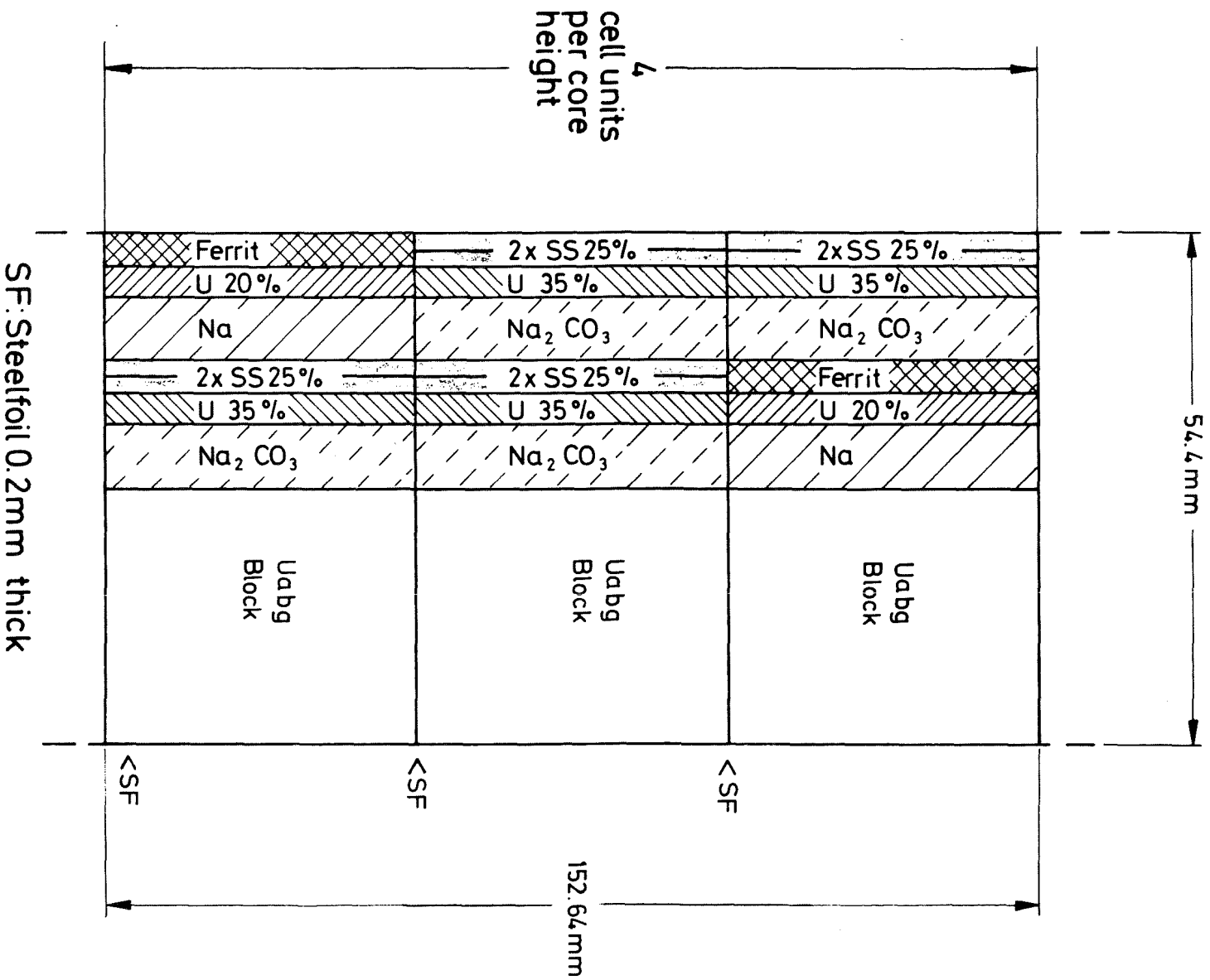


Fig. 2b Cell design of radially half loaded elements.  
Critical core SNEAK 9C1

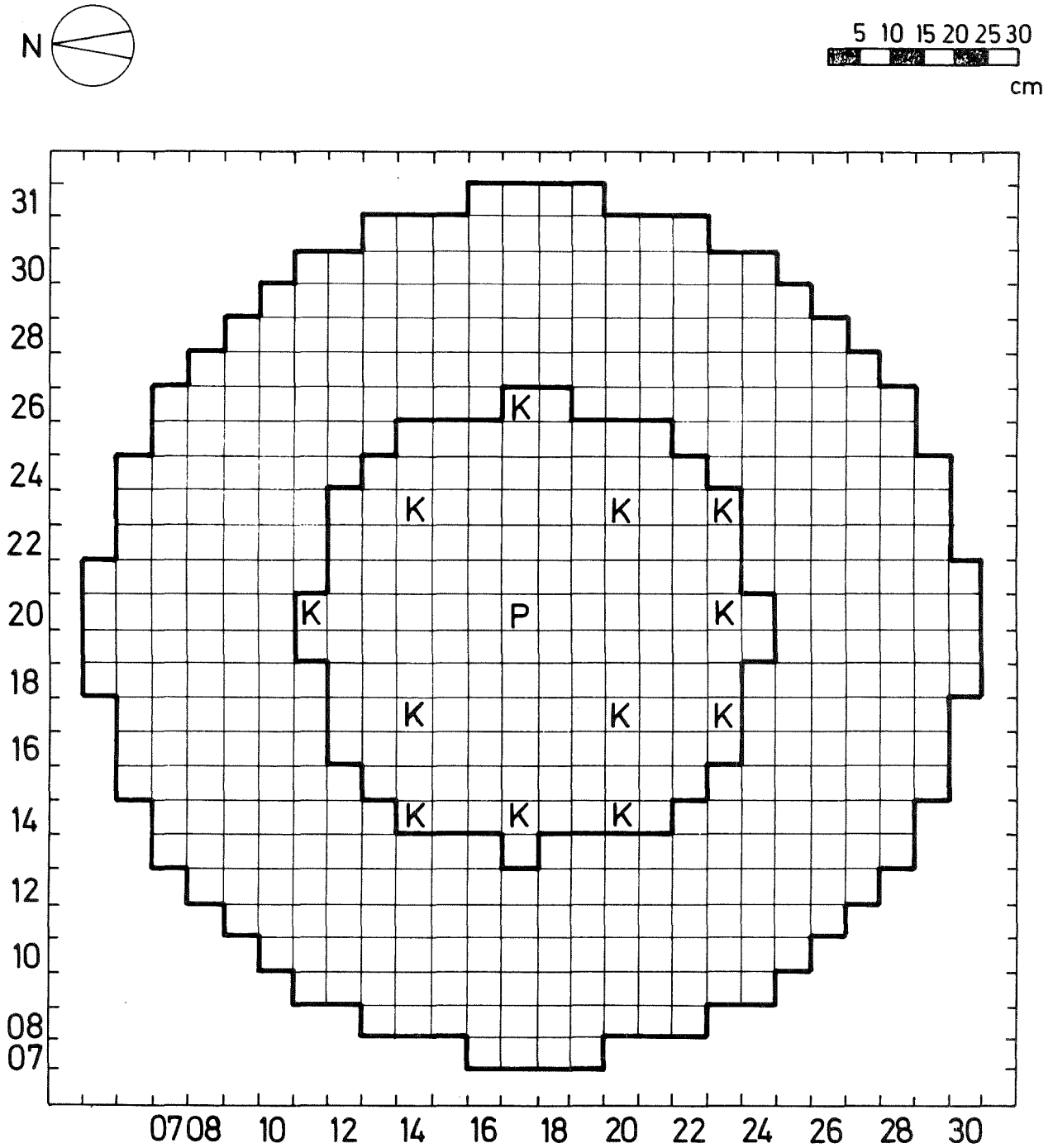
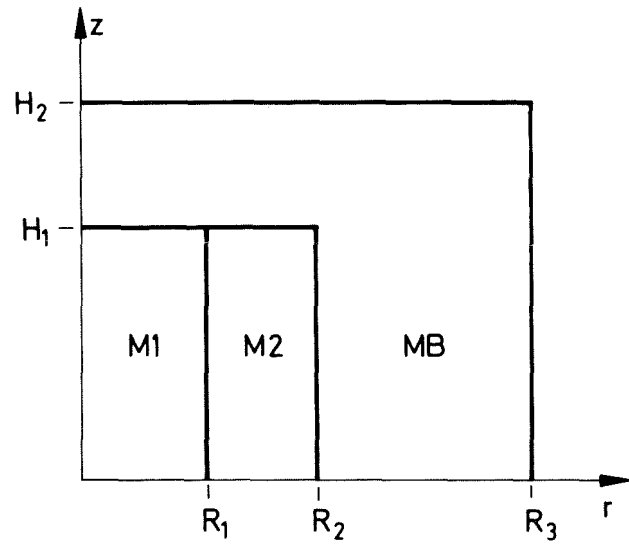


Fig. 3a Gross section of SNEAK 9C-2 critical experiment

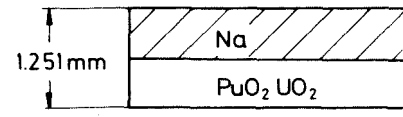
K SNEAK control element  
P Position for pile oscillator



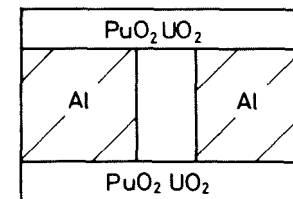
$R_1 = 19.41 \text{ cm}$        $H_1 = 30.02 \text{ cm}$   
 $R_2 = 36.19 \text{ cm}$        $H_2 = 60.50 \text{ cm}$   
 $R_3 = 68.63 \text{ cm}$   
 $M_i$  Mixture numbers

Fig. 3b Geometrical model for r-z diffusion calculation

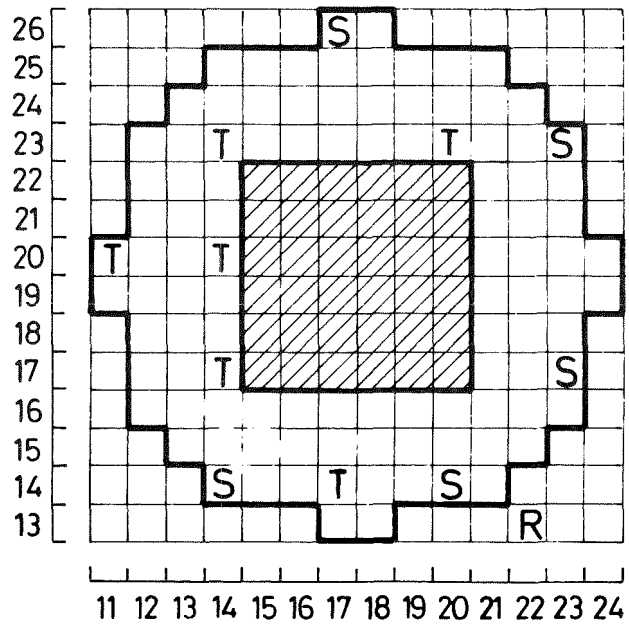
Fig. 4 Cells of SNEAK 9C-2



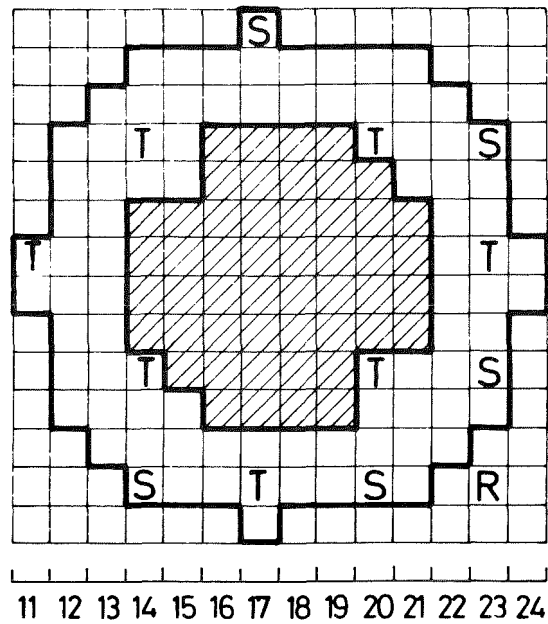
Normal cell



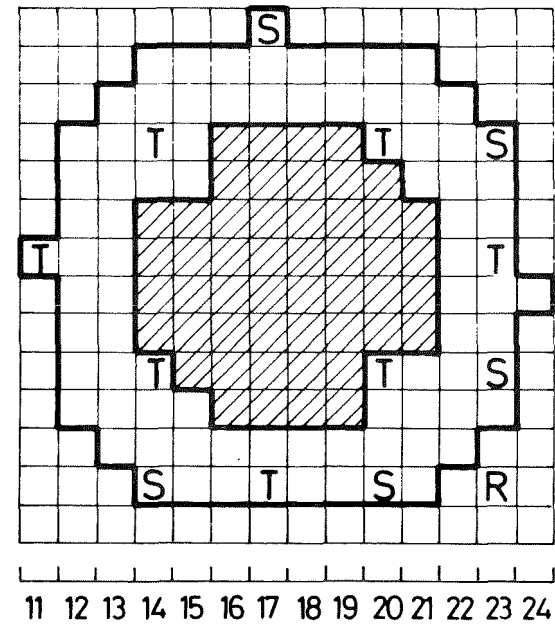
Window cell



PO - S



PO - Z



C - Zone



T : SNEAK Shim rod  
 S : SNEAK Safety rod  
 R : SNEAK Regulating rod



Fig.5 Cross sections of 9C-2 assemblies with zones of high <sup>240</sup>Pu content

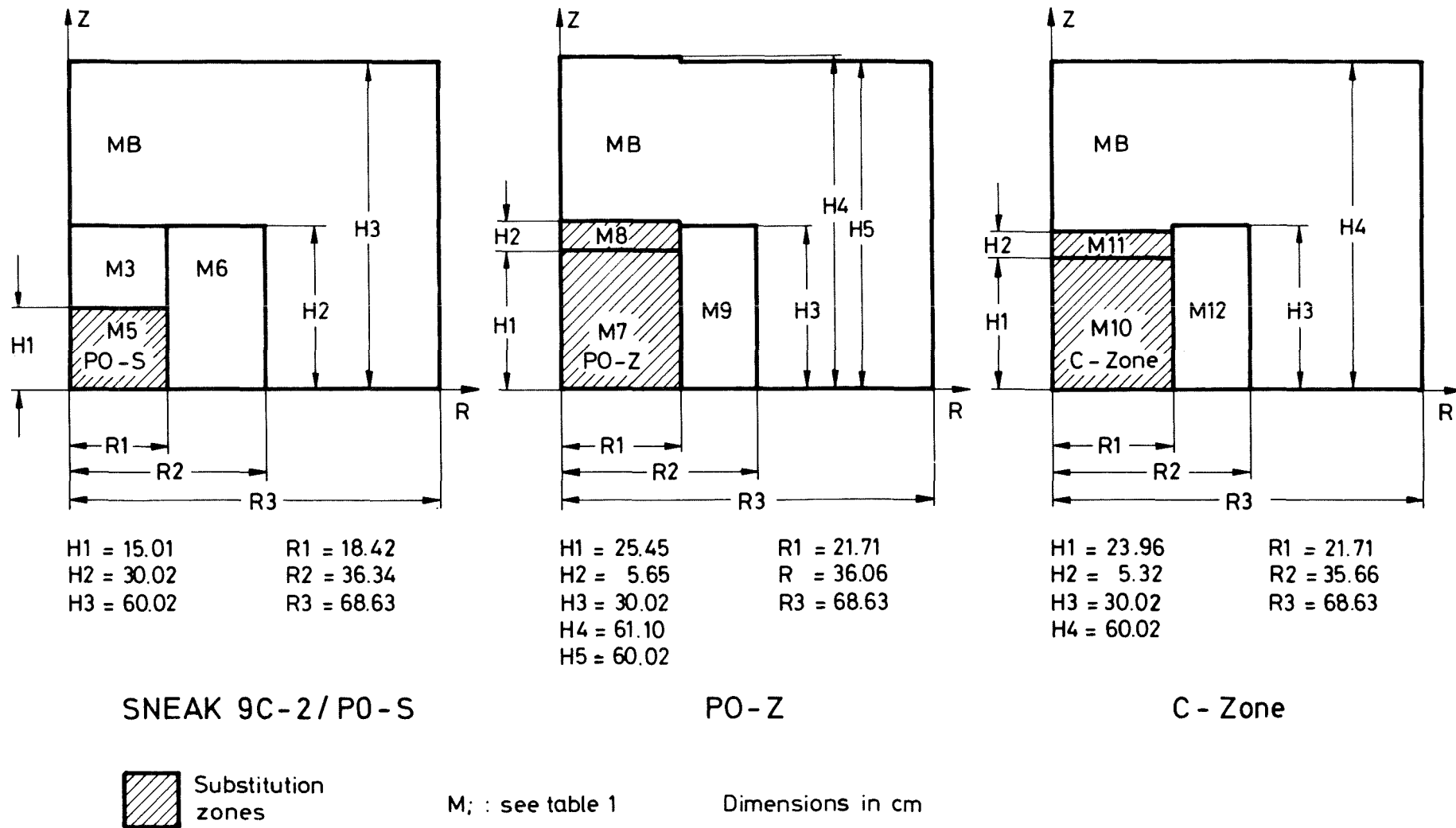
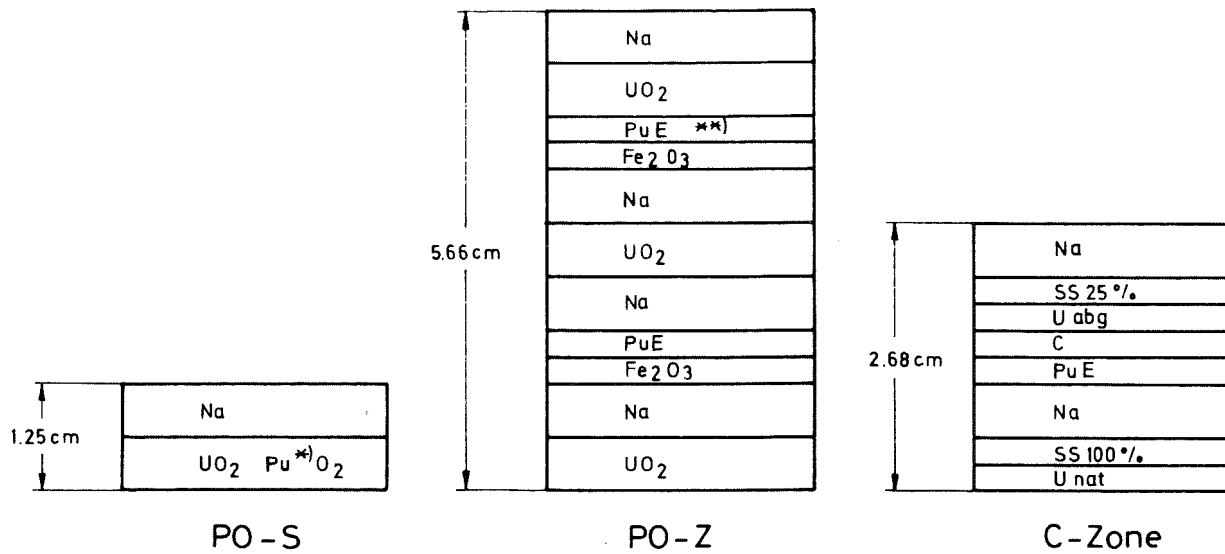


Fig. 6 r - z diagrams of SNEAK 9C-2 assemblies with zones of high  $^{240}\text{Pu}$  - content

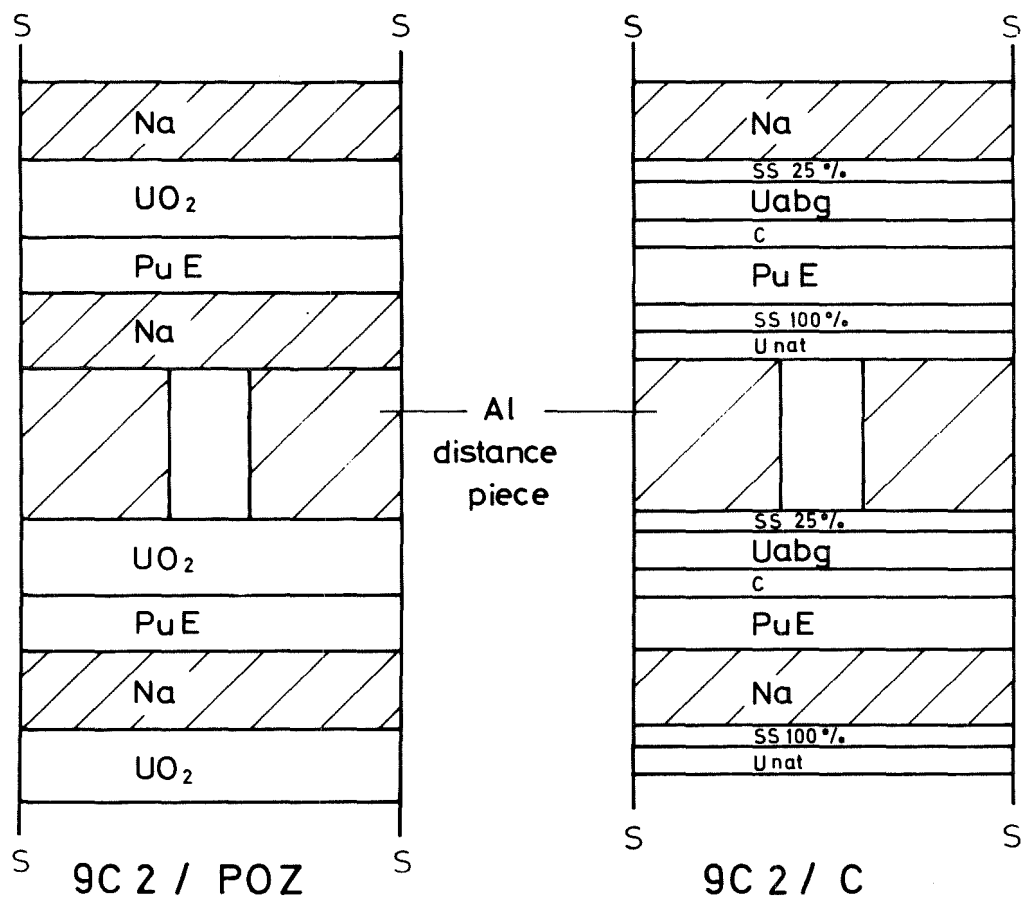


\* ) 18 % Pu 240 ( SNEAK stock )

\*\* ) ZEBRA Pu Platelet

Fig.7a Cell structure of zones with high  $^{240}\text{Pu}$  content in SNEAK 9C 2

Fig. 7b Window cells for radial channel elements



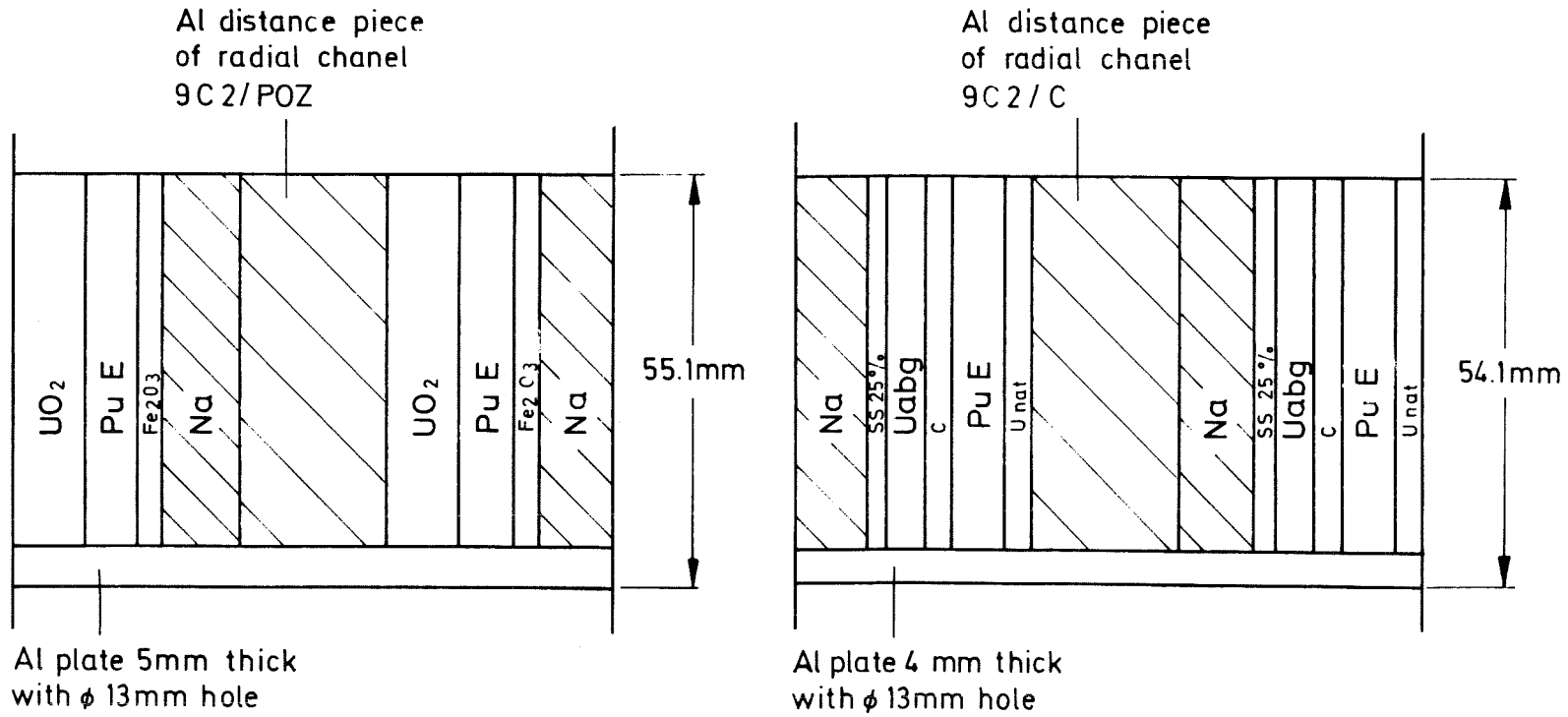


Fig.7c window cells for axial channel elements

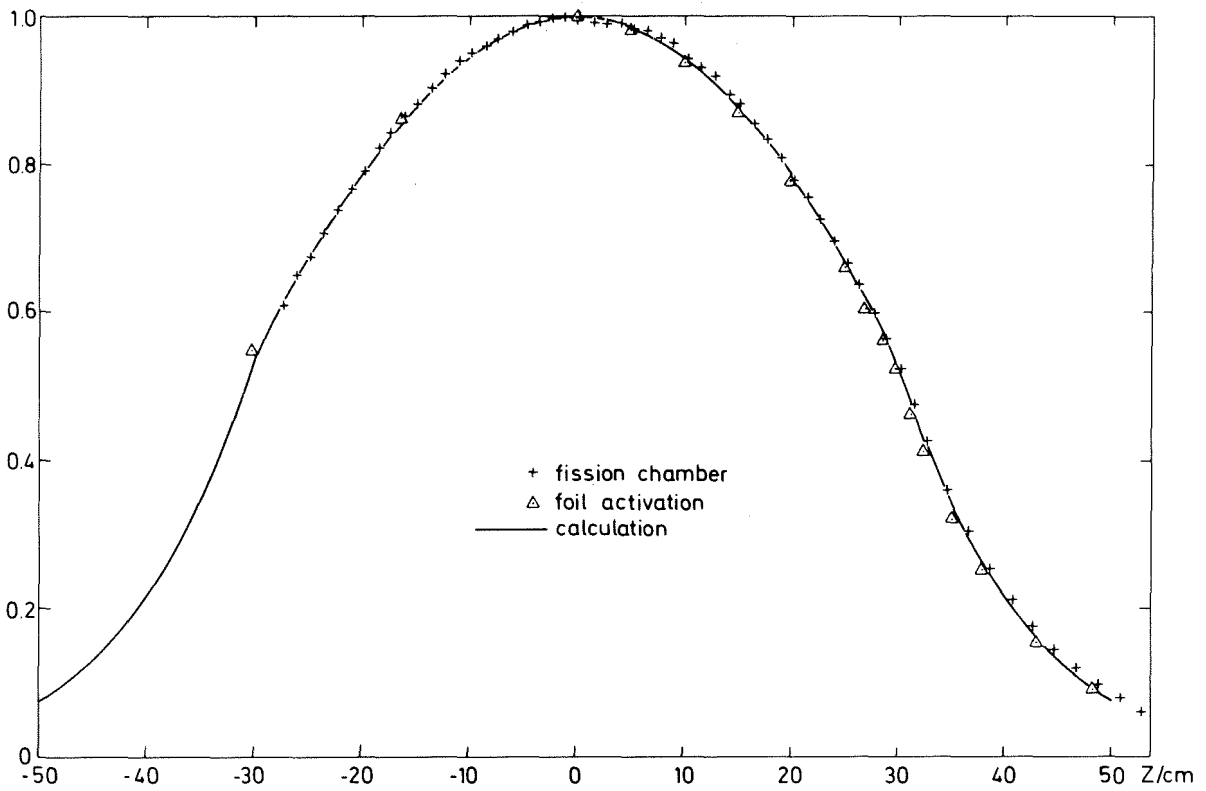


Fig.8a Axial fission rate traverse of  $^{235}\text{U}$  in SNEAK 9C2

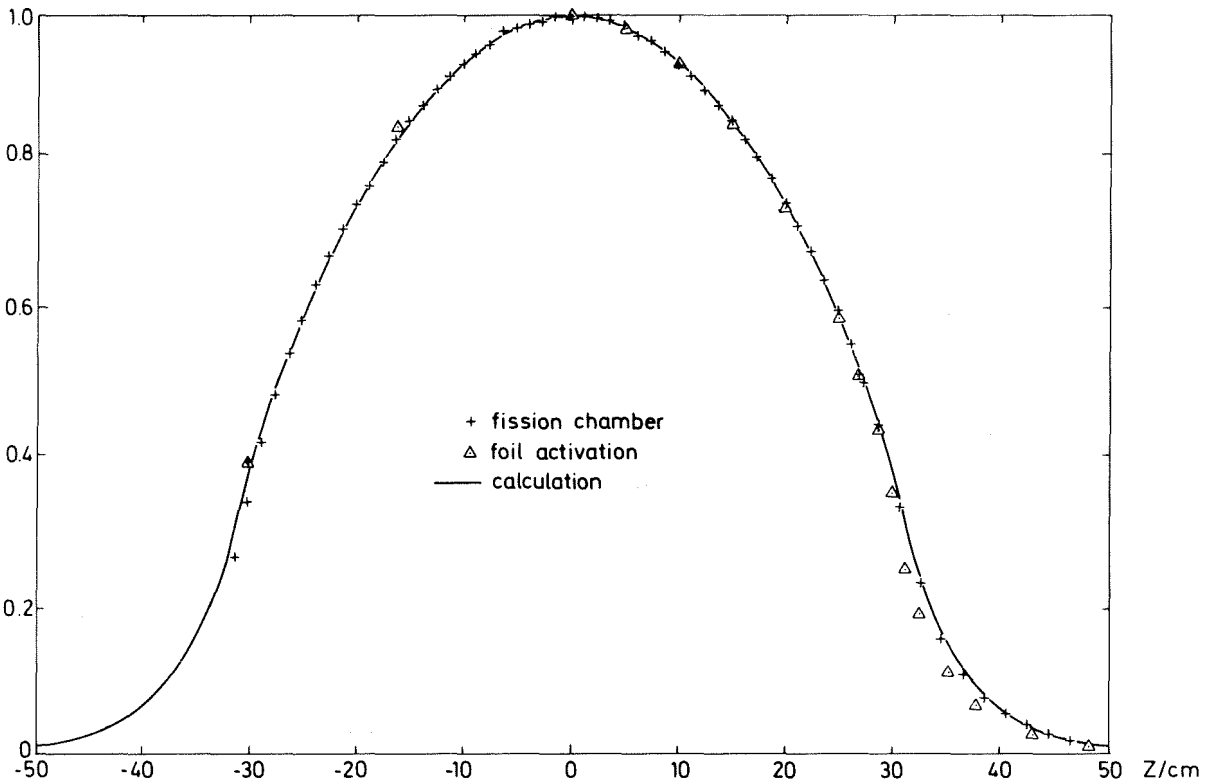


Fig.8b. Axial fission rate traverse of  $^{228}\text{U}$  in SNEAK 9C2

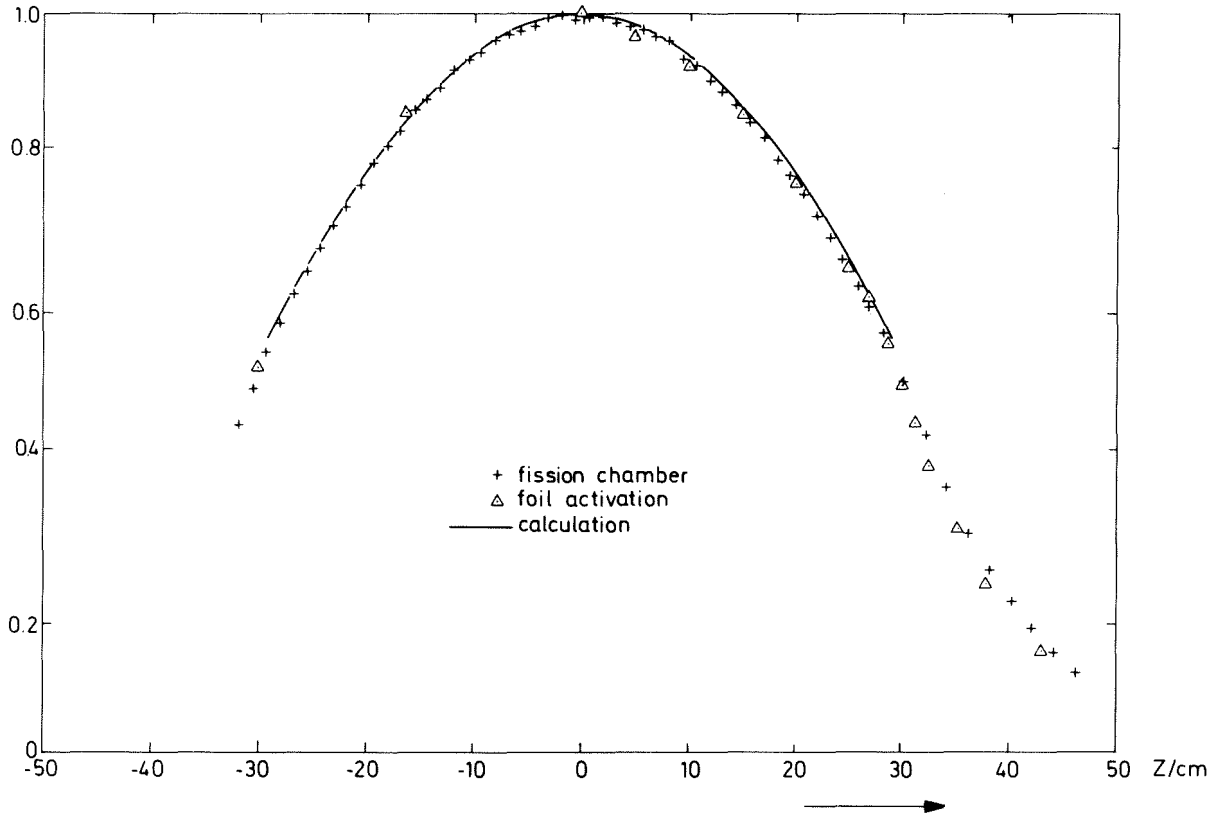


Fig. 8c Axial fission rate traverse of  $^{239}\text{Pu}$  in SNEAK 9C2

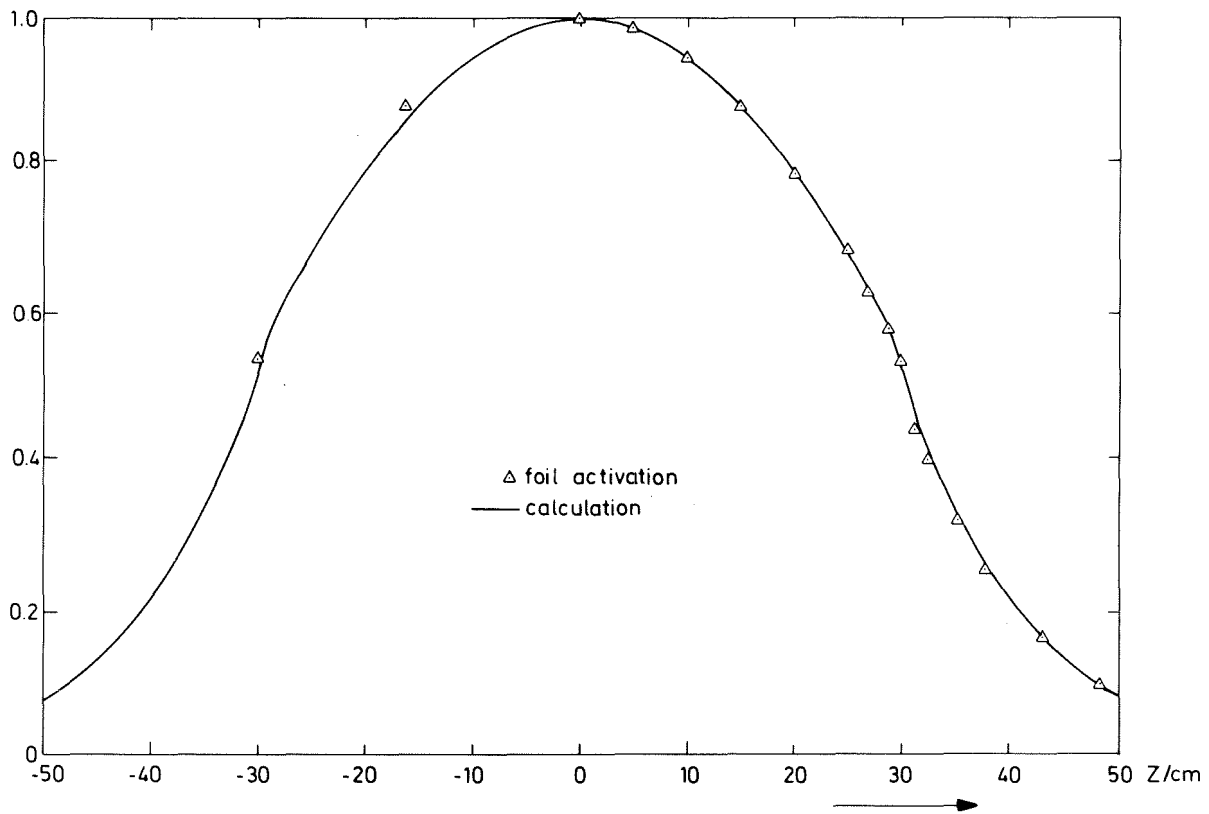


Fig. 8d. Axial capture rate traverse of  $^{238}\text{U}$  in SNEAK 9C2

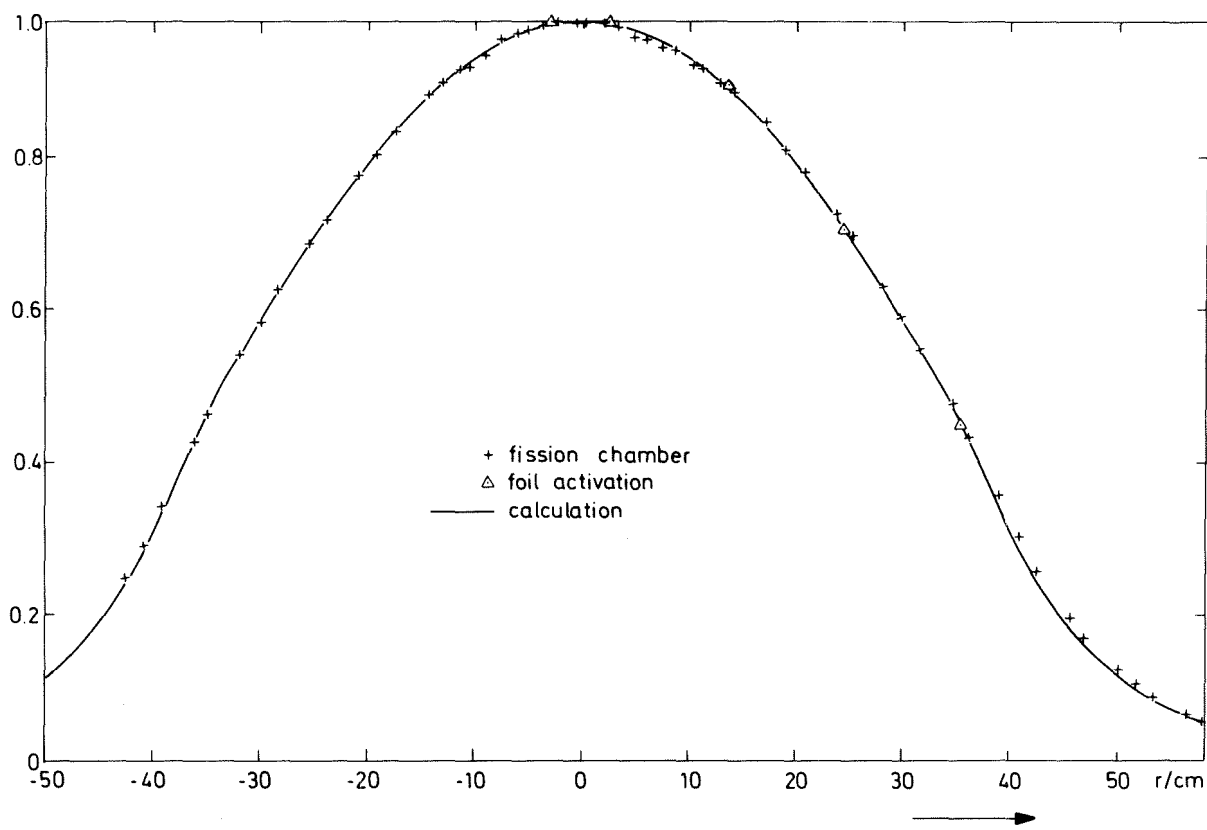


Fig. 9a Radial fission rate traverse of  $^{235}\text{U}$  in SNEAK 9C 2

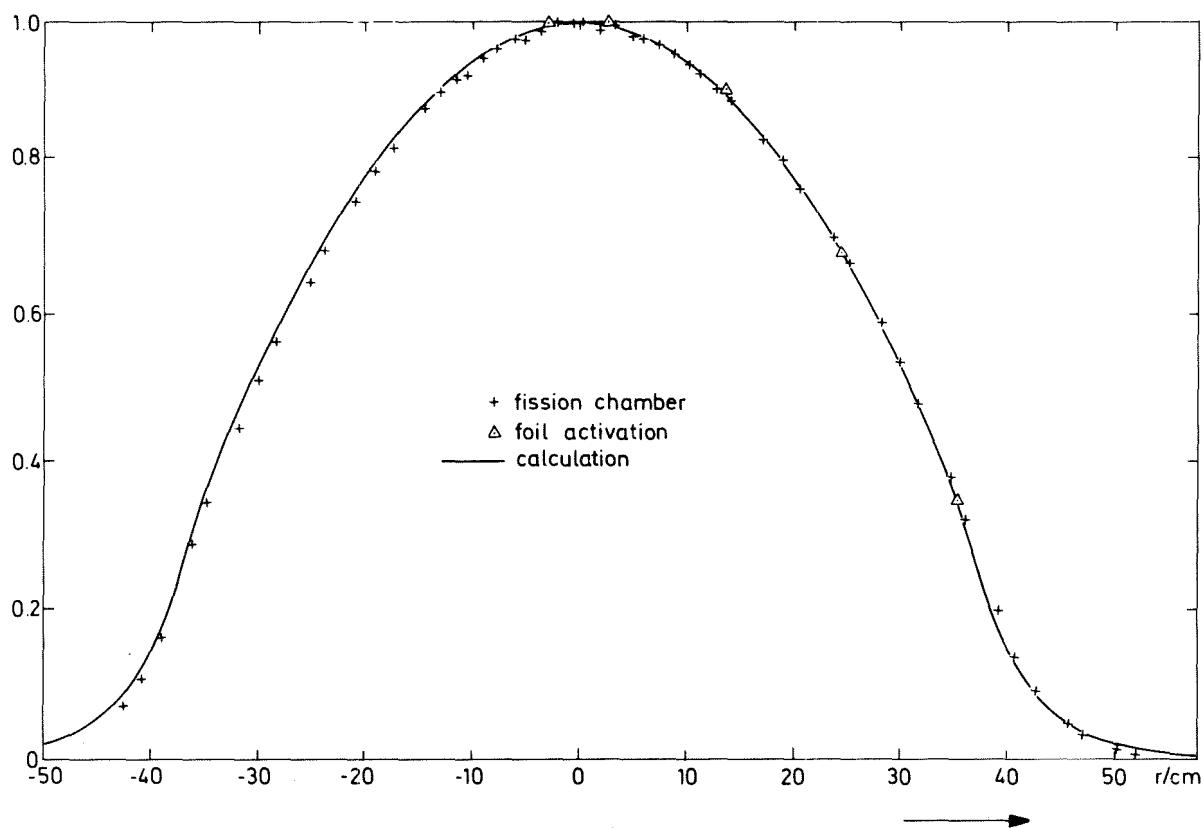


Fig. 9b Radial fission rate traverse of  $^{238}\text{U}$  in SNEAK 9C 2

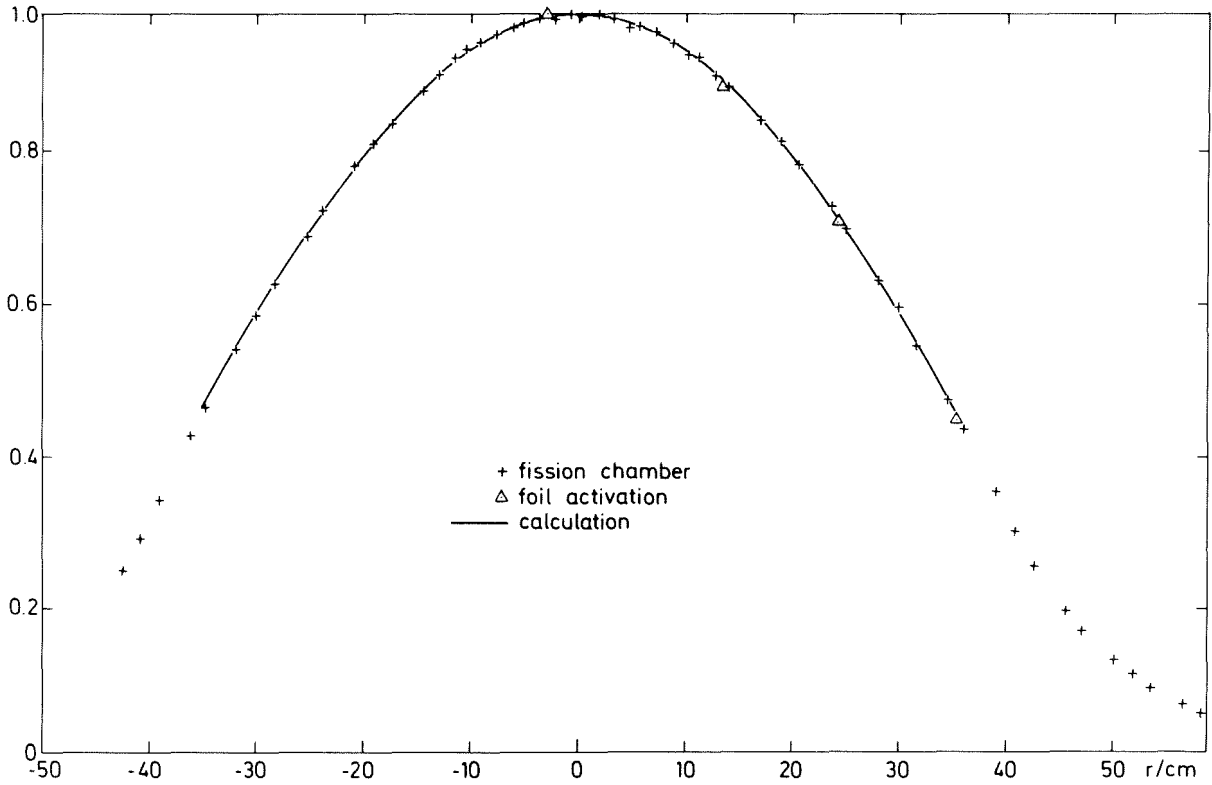


Fig. 9c Radial fission rate traverse of  $^{239}\text{Pu}$  in SNEAK 9C 2

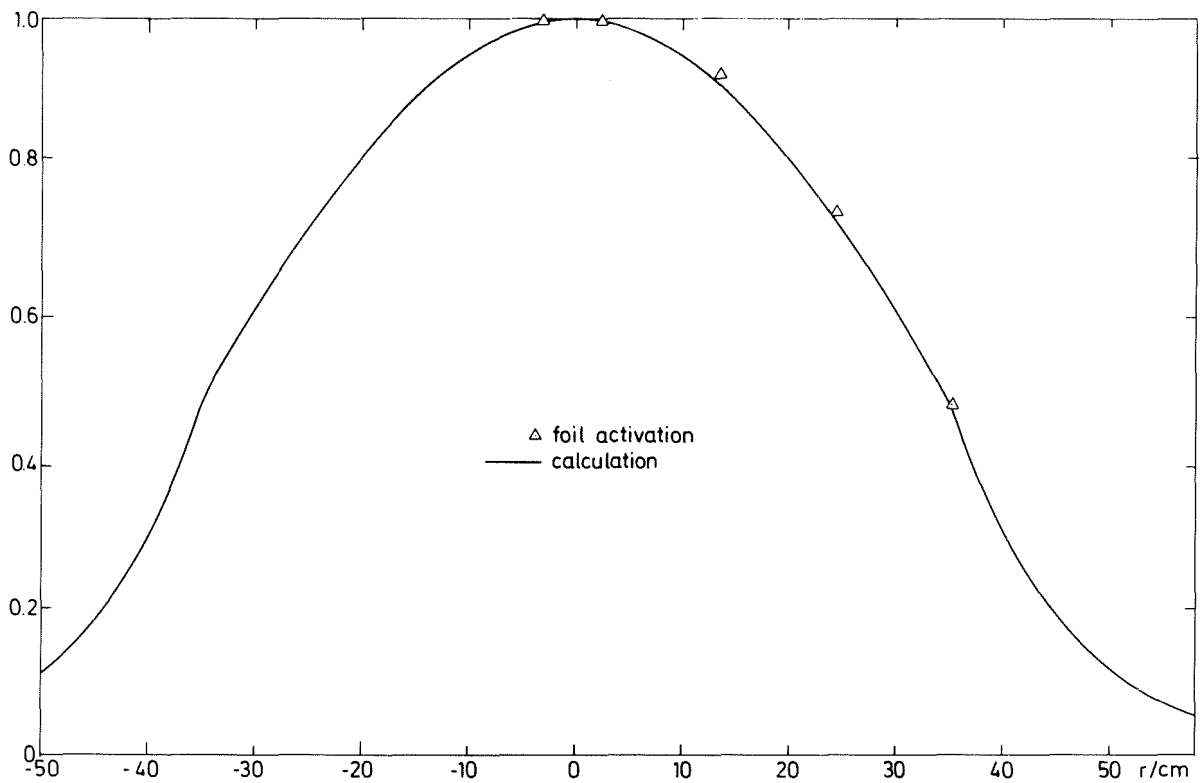


Fig. 9d Radial capture rate traverse of  $^{238}\text{U}$  in SNEAK 9C 2

Fig.10 Fine structure measurement cell in the POZ - zone

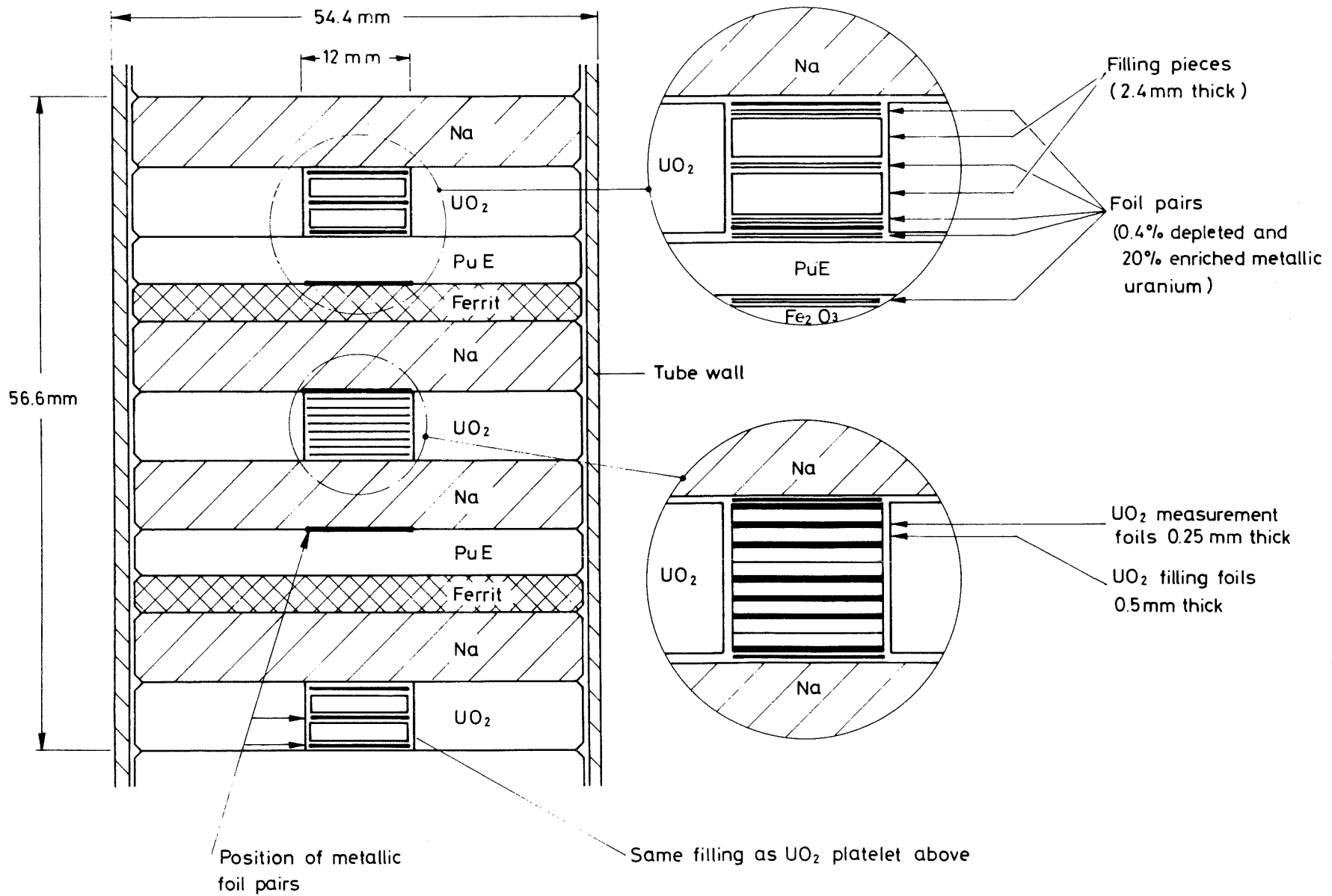




Fig.12  $^{238}\text{U}$  reaction rate fine structures in the 9C 2 cell, normalized to the macroscopic cell average

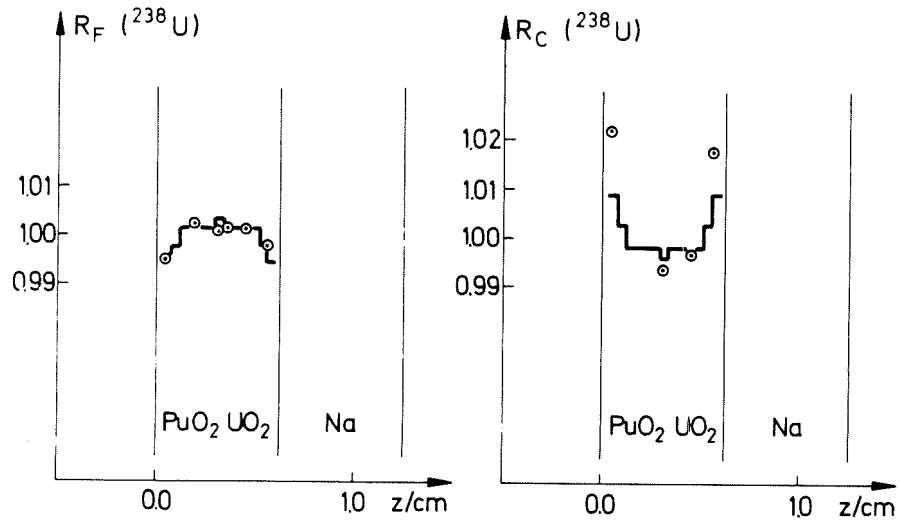


Fig.13  $^{238}\text{U}$  reaction rate fine structures in the 9C 2 / POS cell, normalized to the macroscopic cell average

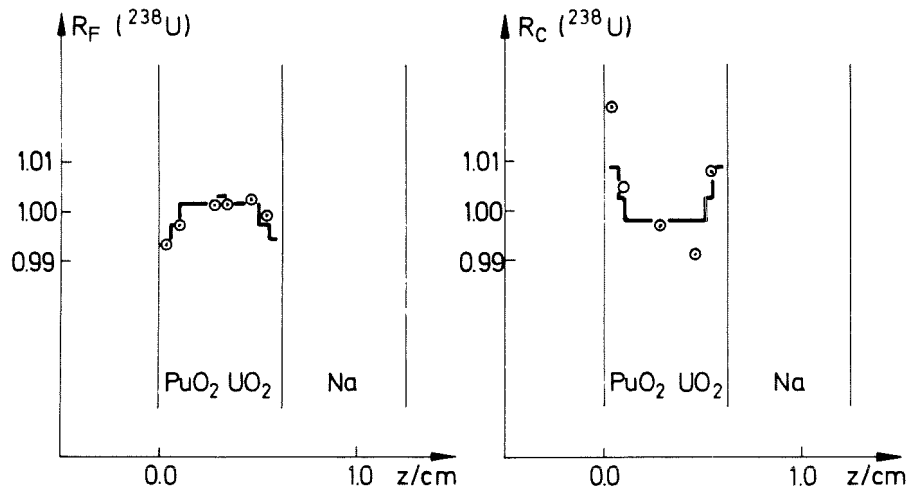


Fig.14a  $^{238}\text{U}$  fission rate fine structure in the 9C 2 / POZ cell , normalized to the macroscopic cell average.

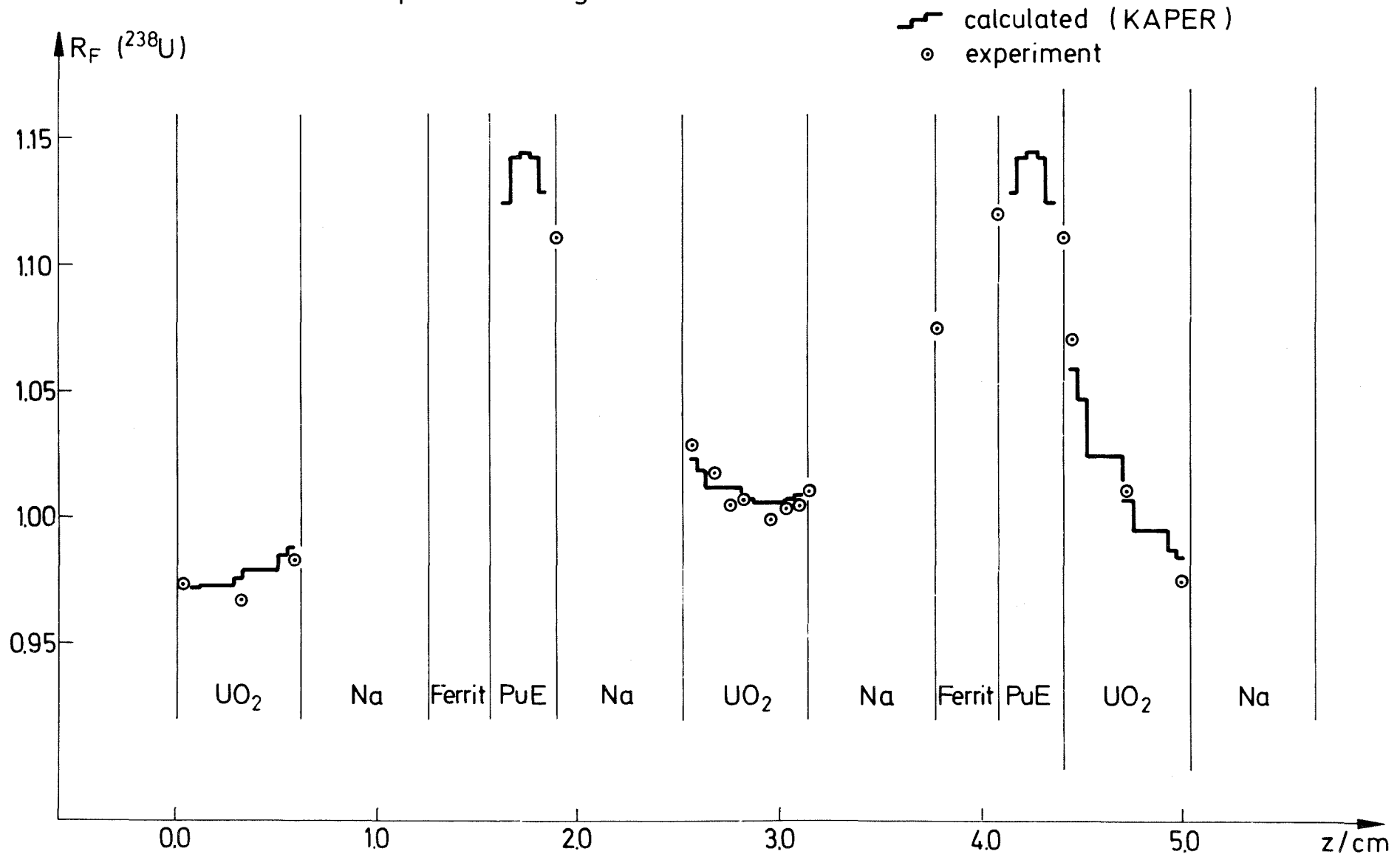


Fig. 14 b  $^{238}\text{U}$  capture rate fine structure in the 9C 2 / POZ cell, normalized to the macroscopic cell average

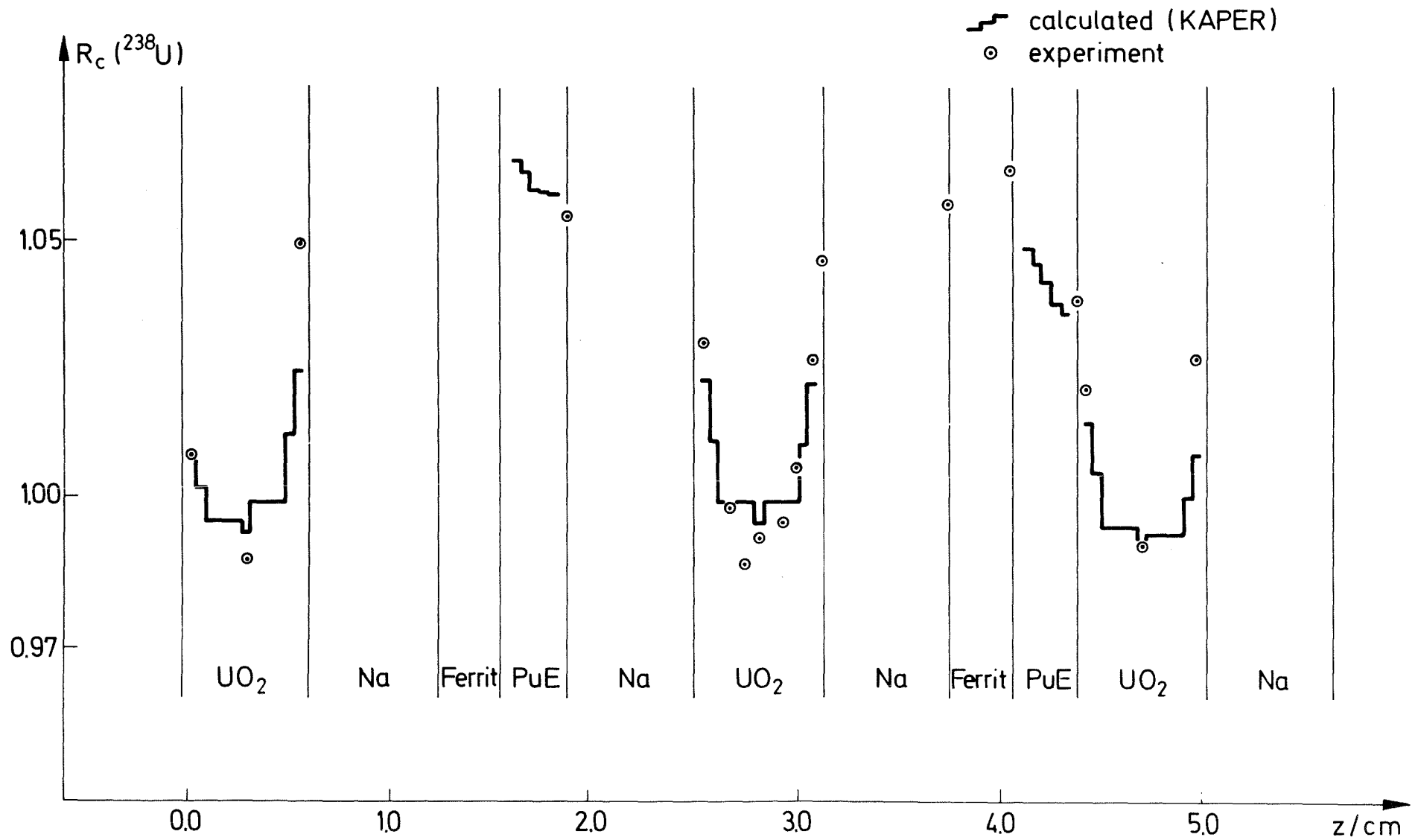


Fig.15  $^{238}\text{U}$  reaction rate fine structure in the 9C 2/C cell, normalized to the macroscopic cell average

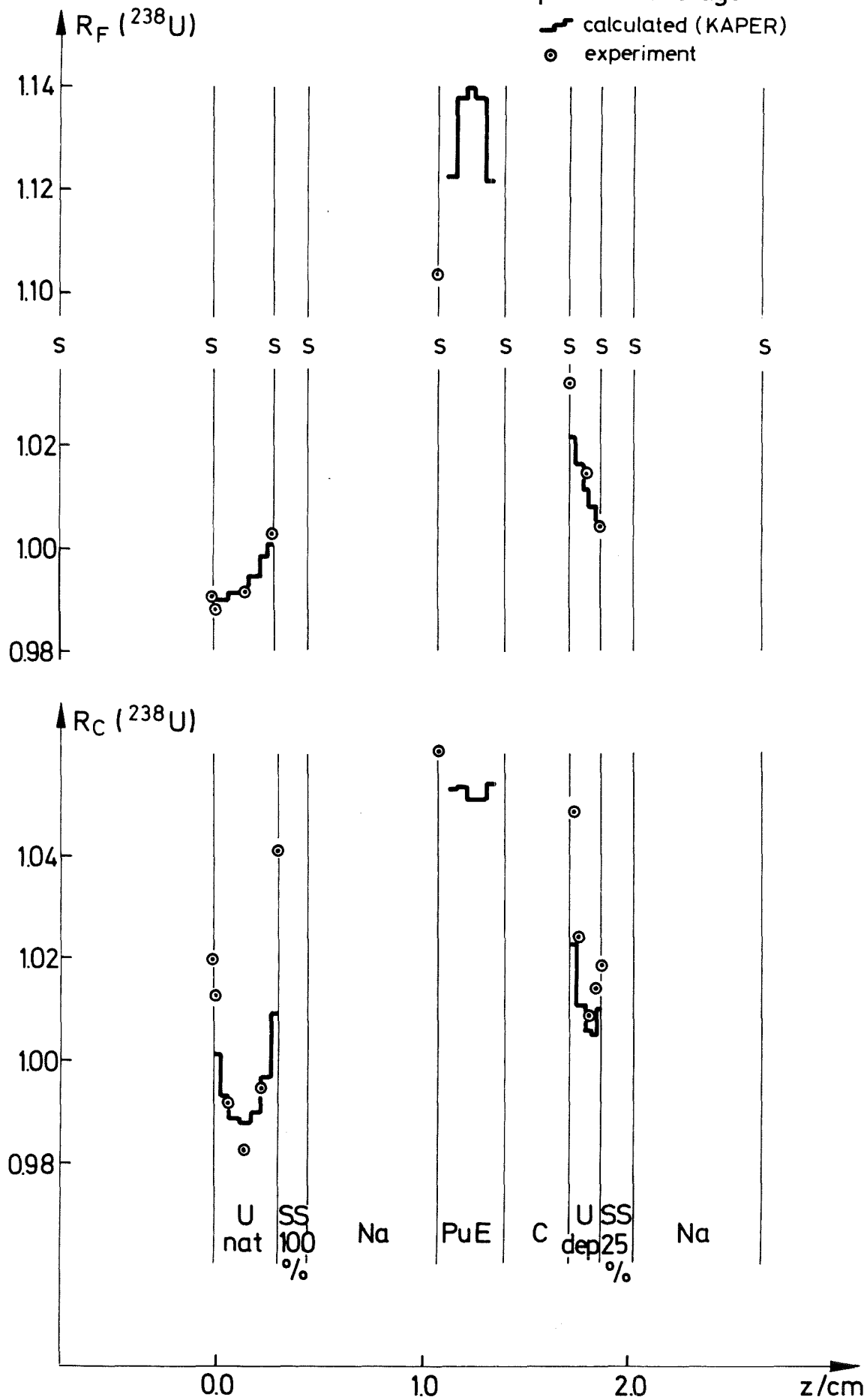


Fig.16 Experimental arrangement of miniature chamber measurements in SNEAK 9C-2

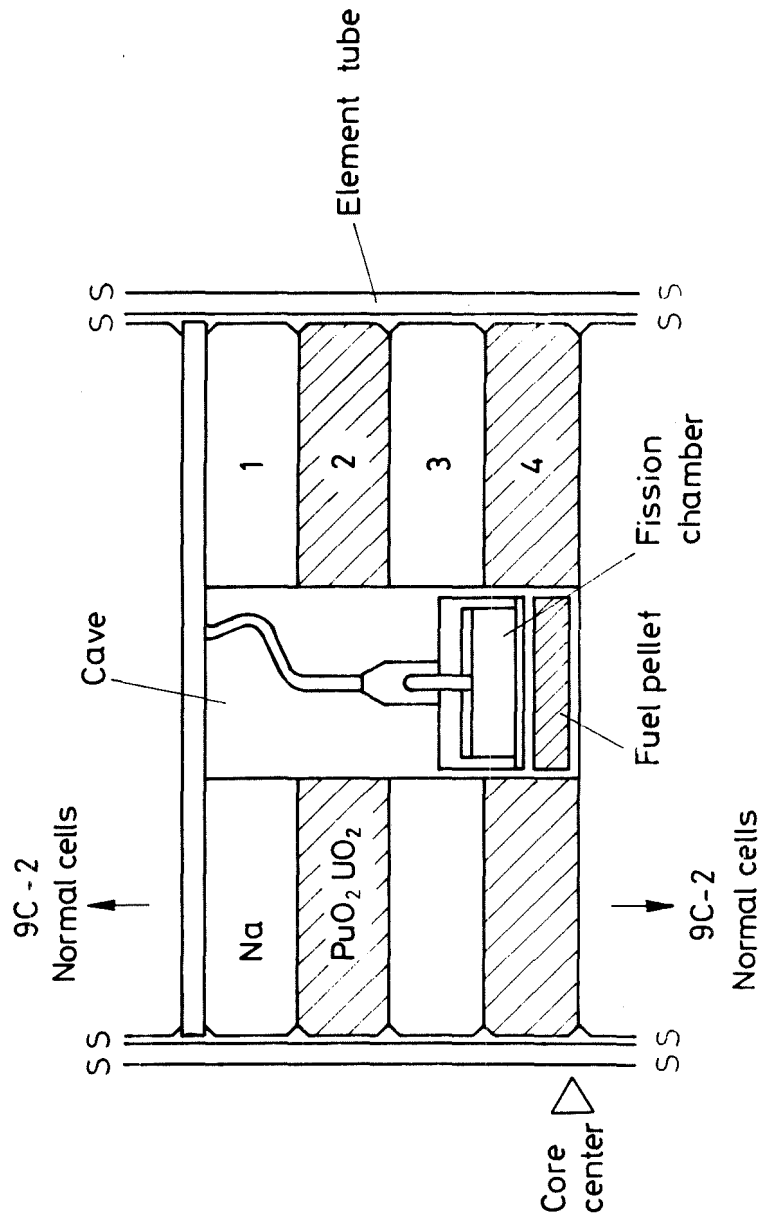
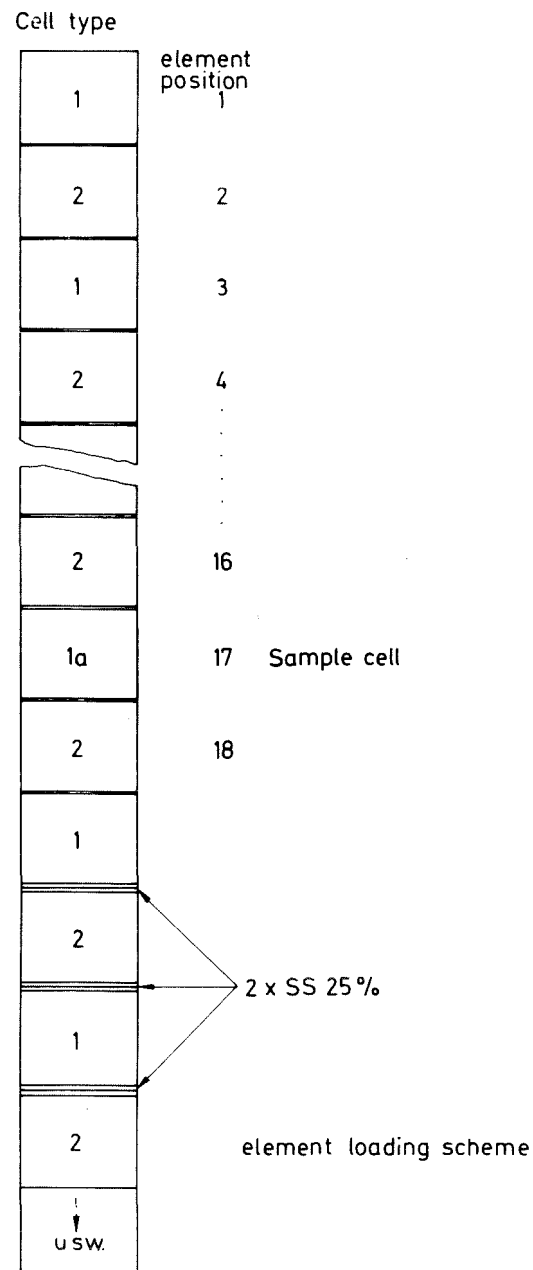
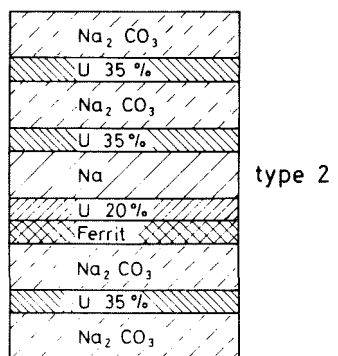
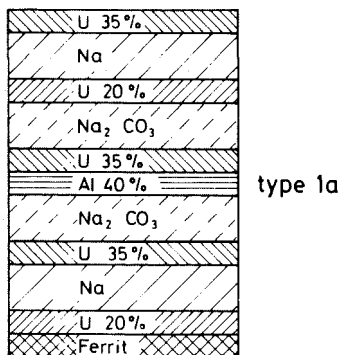
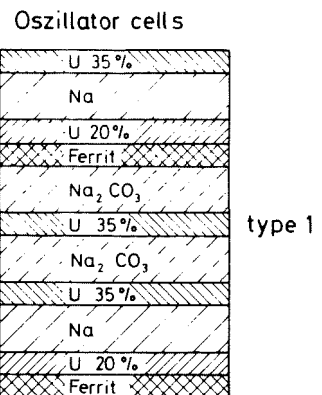
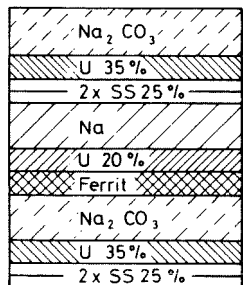


Fig.17  
Oszillator cell and element configuration in SNEAK 9C 1





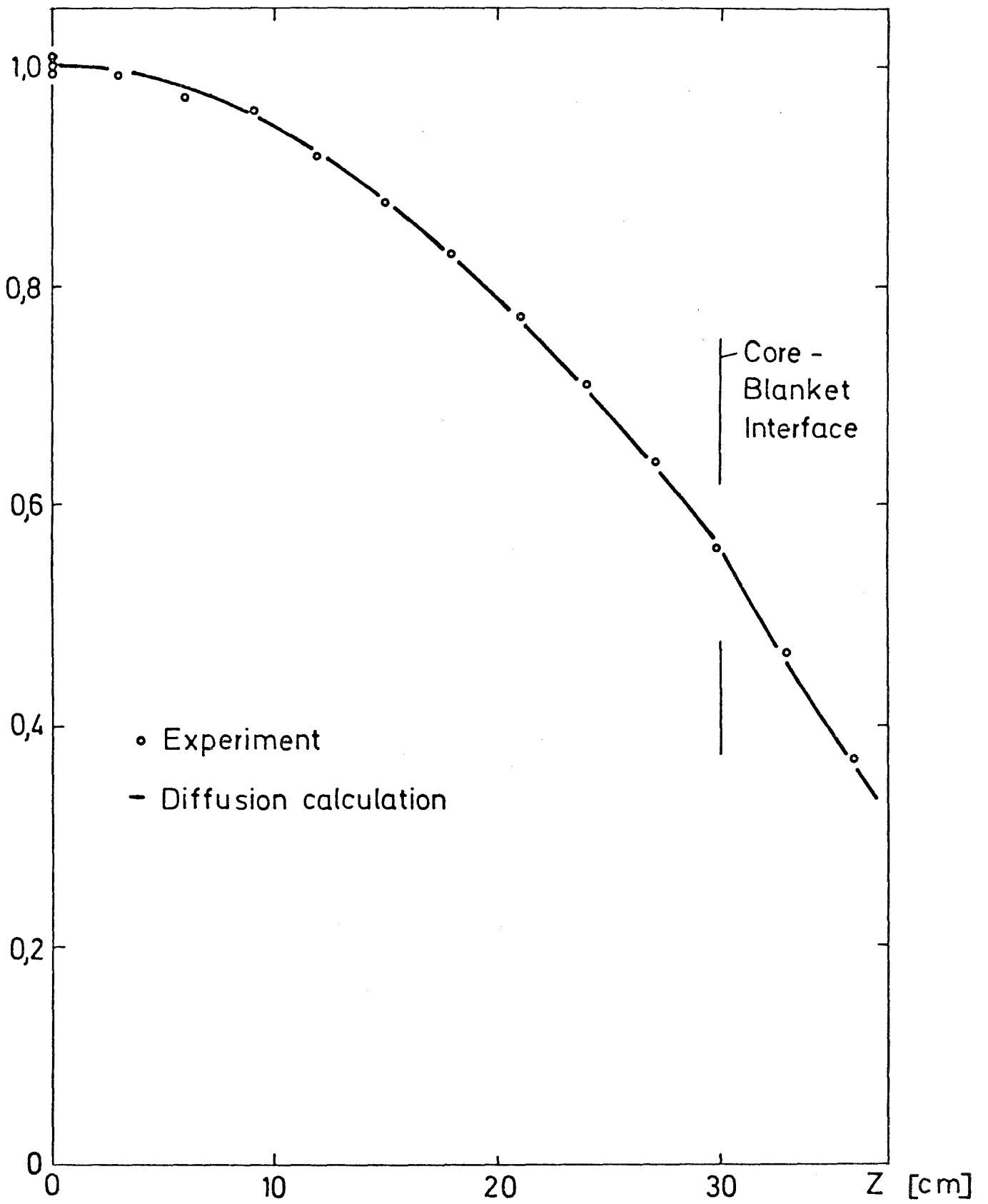


Fig. 19 Axial importance traverse in SNEAK 9C 2